International Journal of Nanomedicine

Dovepress

open access to scientific and medical research

Open Access Full Text Article

ORIGINAL RESEARCH

# Green Synthesis of Zinc Oxide Nanoparticles from *Althaea officinalis* Flower Extract Coated with Chitosan for Potential Healing Effects on Diabetic Wounds by Inhibiting TNF-α and IL-6/IL-1β Signaling Pathways

Sammar Fathy Elhabal[1], Nashwa Abdelaal[2], Saeed Abdul Kareem Saeed Al-Zuhairy[3], Mohamed Fathi Mohamed Elrefai[4,5], Ahmed Mohsen Elsaid Hamdan[6], Mohamed Mansour Khalifa[7], Sandra Hababeh[8], Mohammad Ahmad Khasawneh[9], Gehad M Khamis[10], Jakline Nelson[11], Passant M Mohie[10], Rania A Gad[12], Amira Rizk[13], Soad L Kabil[14], Mohamed Kandeel El-Ashery[15,16], Bhaskara R Jasti[17], Nahla A Elzohairy[18,19], Tayseer Elnawawy[20], Fatma E Hassan[21,22], Mohamed A El- Nabarawi[23]

[1]Department of Pharmaceutics and Industrial Pharmacy, Faculty of Pharmacy, Modern University for Technology and Information (MTI), Mokattam, Cairo, Egypt; [2]Department of Integrative Physiology, Baylor College of Medicine, Houston, TX, USA; [3]Department of Pharmacy, Kut University College, Kut, Wasit, Iraq; [4]Department of Anatomy, Histology, Physiology and Biochemistry, Faculty of Medicine, The Hashemite University, Zarqa, Jordan; [5]Department of Anatomy and Embryology, Faculty of Medicine, Ain Shams University, Cairo, Egypt; [6]Department of Pharmacy Practice, Faculty of Pharmacy, University of Tabuk, Tabuk, Saudi Arabia; [7]Department of Human Physiology, Faculty of Medicine, Cairo University, Cairo, Egypt; [8]Department of Pharmaceutics, College of Pharmacy, King Saud University, Riyadh, Saudi Arabia; [9]Department of Chemistry, College of Science U.A.E. University, Al-Ain, United Arab Emirates; [10]Department of Clinical Pharmacology, Faculty of Medicine, Alexandria University, Alexandria, Egypt; [11]Department of Microbiology and Immunology, Faculty of Pharmacy, Nahda University, Beni-Suef, Egypt; [12]Department of Pharmacology and Toxicology, Faculty of Pharmacy, Nahda University, Beni-Suef, Egypt; [13]Food Science and Technology Department, Faculty of Agricultural, Tanta University, Tanta, Egypt; [14]Department of Clinical Pharmacology, Faculty of Medicine, Zagazig University, Zagazig, Egypt; [15]Pharmaceutical Chemistry Department, Faculty of Pharmacy, Cairo University, Cairo, Egypt; [16]Medicinal Chemistry Department, Faculty of Pharmacy, King Salman International University, Ras-Sedr, South Sinai, Egypt; [17]Department of Pharmaceutics and Medicinal Chemistry, Thomas J. Long School of Pharmacy, University of the Pacific, Stockton, CA, USA; [18]Air Force Specialized Hospital, Cairo, Egypt; [19]Department of Microbiology and Immunology, Faculty of Pharmacy, Modern University for Technology and Information (MTI), Mokattam, Cairo, Egypt; [20]Department of Pharmaceutics, Egyptian Drug Authority, Cairo, Egypt; [21]Medical Physiology Department, Faculty of Medicine, Cairo University, Giza, Egypt; [22]General Medicine Practice Program, Department of Physiology, Batterjee Medical College, Jeddah, Saudi Arabia; [23]Department of Pharmaceutics and Industrial Pharmacy, Faculty of Pharmacy, Cairo University, Cairo, Egypt

Correspondence: Sammar Fathy Elhabal, Email Sammar.Fathy@pharm.mti.edu.eg; sammar_fathy2007@yahoo.com; Mohamed A El- Nabarawi, Email mohamed.elnabarawi@pharm.cu.edu.eg

**Background:** Diabetes Mellitus is a multisystem chronic pandemic, wound inflammation, and healing are still major issues for diabetic patients who may suffer from ulcers, gangrene, and other wounds from uncontrolled chronic hyperglycemia. *Marshmallows or Althaea officinalis (A.O.)* contain bioactive compounds such as flavonoids and phenolics that support wound healing via antioxidant, anti-inflammatory, and antibacterial properties. Our study aimed to develop a combination of eco-friendly formulations of green synthesis of ZnO-NPs by *Althaea officinalis* extract and further incorporate them into 2% chitosan (CS) gel.

**Method and Results:** First, develop eco-friendly green Zinc Oxide Nanoparticles (ZnO-NPs) and incorporate them into a 2% chitosan (CS) gel. In-vitro study performed by UV-visible spectrum analysis showed a sharp peak at 390 nm, and Energy-dispersive X-ray (EDX) spectrometry showed a peak of zinc and oxygen. Besides, Fourier transforms infrared (FTIR) was used to qualitatively validate biosynthesized ZnO-NPs, and transmission electron microscope (TEM) showed spherical nanoparticles with mean sizes of 76 nm and Zeta potential +30mV. The antibacterial potential of A.O.-ZnO-NPs-Cs was examined by the diffusion agar method against Gram-positive (*Staphylococcus aureus* and *Bacillus subtilis*) and Gram-negative bacteria (*Escherichia coli* and *Pseudomonas aeruginosa*). Based on the zone of inhibition and minimal inhibitory indices (MIC). In addition, an in-silico study investigated the binding affinity of *A.O.* major components to the expected biological targets that may aid wound healing. *Althaea Officinalis*, A.O-ZnO-NPs group showed reduced

Received: 17 January 2024
Accepted: 14 March 2024
Published: 27 March 2024

downregulation of IL-6, IL-1β, and TNF-α and increased IL-10 levels compared to the control group signaling pathway expression levels confirming the improved anti-inflammatory effect of the self-assembly method. *In-vivo study* and histopathological analysis revealed the superiority of the nanoparticles in reducing signs of inflammation and wound incision in rat models.

**Conclusion:** These biocompatible green zinc oxide nanoparticles, by using *Althaea Officinalis* chitosan gel ensure an excellent new therapeutic approach for quickening diabetic wound healing.

**Keywords:** wound healing, antimicrobial, antioxidant, *Staphylococcus aureus*, *Bacillus subtilis*, *Escherichia coli*, *Pseudomonas aeruginosa*, chitosan, wound concentration, wound incision

**Graphical Abstract**

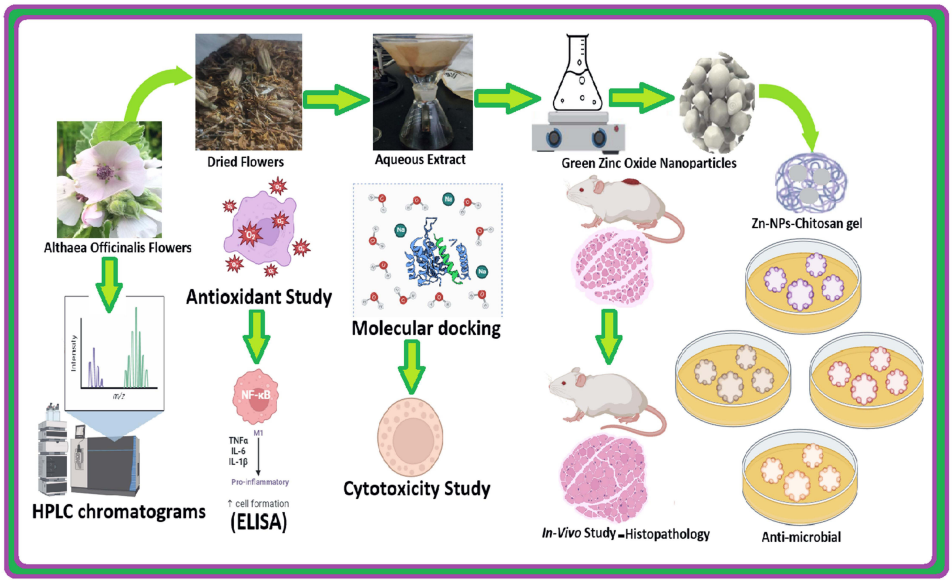


## Introduction

The advancement of dependable and environmentally friendly techniques to produce metallic nanoparticles (NPs) holds significant importance in the domains of nanobiotechnology and nanoscience. While there are several approaches to synthesizing NPs, many are costly and harmful to the environment. This has led to a growing demand for nontoxic and eco-friendly processes that can produce NPs with desired characteristics. One promising approach is to utilize natural processes involving microbes, enzymes, and biological systems by leveraging these natural processes, it is possible to create green nanoparticles as a substitute for physical and chemical techniques.[1–3]

Plants include a variety of proteins and phytochemicals that contribute to the creation of metal and metal oxide nanoparticles, including copper, zinc, silver, and gold. Plants, that are rich in antioxidants, are perfect candidates, for formulating nanoparticles. Among metal oxide nanoparticles used in biomedical applications, zinc oxide nanoparticles (ZnO-NPs) are widely used for wound healing, antibacterial properties, anti-inflammatory effects, and enhancement of farm animal growth, immunological response, and reproductive status. ZnO-NPs have shown potential in various skin therapies due to their ability to promote wound healing, reduce inflammation, and facilitate tissue granulation at the wound site.[4–6]

*Althaea Officinalis* (A.O.), or marshmallow, is a member of the Malvaceae family of plants. It is grown all over the world but is native to Europe, the US, and some regions of Asia. Many ailments, including wound incisions, irritation of the oral and pharyngeal mucosa, gastritis, skin burns, insect bites, catarrh, gastrointestinal problems, urinary tract complaints, inflammation, abscesses, burns, constipation, and diarrhea, have historically been treated with *A.O*. It has been previously reported that *A.O*. possesses antibacterial, anti-inflammatory, immunomodulatory, demulcent, calming,

antitussive, and nutraceutical properties.[7–9] The aqueous extract of *Althaea Officinalis* contains important compounds like flavonoid glycosides, phenolic acids, mucilage, carbohydrates, tannins, and flavonoids, which contribute to its high antioxidant activity.[10]

Chitosan, a biopolymer, has gained significant attention in wound healing due to its biocompatibility, biodegradability, non-toxicity, and antibacterial properties. Chitosan (CS) and its derivatives can be easily processed into different forms (beads, gels, foams, membranes) and are adaptable and promising for wound dressings.[11,12] Secondary natural metabolites present in chitosan-based materials can act as antibacterial and anti-inflammatory agents, promoting the healing process. Materials based on CS have also been thoroughly researched for use in medication delivery systems. They can cling to mucosal tissues, shield unstable drug molecules, and enhance the absorption of particular medications since they are biocompatible. Systems based on CS have been investigated for gene delivery, topical application, oral administration, colon-targeted drug delivery, and cancer treatment. Chitosan's primary amino groups make it soluble in diluted acidic solutions, making it suitable for oral delivery of anticancer drugs. CS exhibits strong anticancer effects by inhibiting tumor-induced angiogenesis, tumor metastasis, and tumor cell proliferation.[12,13] Combined with therapeutic metal ions, chitosan-based systems can synergistically reduce tumor cell proliferation, shrink tumors, and enhance the effectiveness of chemotherapy. CS can also stimulate innate immune responses, particularly by promoting communication between dendritic cells and natural killer cells, which suggests its potential in anticancer treatments. Over the past decade, there has been a significant increase in research exploring the use of CS and its derivatives in tissue engineering, drug delivery systems, wound healing, antimicrobial applications, and cancer treatment.[12]

Overall, the synthesis of metallic nanoparticles using environmentally friendly methods is crucial in nanobiotechnology and nanoscience[14,15].Natural processes involving microbes, enzymes, and biological systems show promise for creating green nanoparticles. *Althaea Officinalis* and its constituents, such as phenolics and flavonoids, offer potential therapeutic benefits due to their antibacterial, anti-inflammatory, and HMGB1 inhibitory properties. Plant-based materials like CS are versatile and have applications in wound healing, drug delivery systems, and cancer treatments.[1]

This work is aimed to explore the potential of combining eco-friendly green synthesis ZnO-NPs by using *A.O* aqueous extract and coated by CS gel, the formulation can provide synergistic effects that enhance wound healing. The ZnO-NPs contribute antibacterial and anti-inflammatory properties, while the *Althaea officinalis* extract offers antioxidant and anti-inflammatory effects. CS gel functions as a vehicle for the delivery of the formulated nanoparticles and the incorporated aqueous extract, offering a safe and supportive environment for wound healing. Their efficacy in wound healing was evaluated using in vitro, in vivo, histological assessments, and antimicrobial characterization in silico.

# Materials and Methods

## Chemical, and Reagent Kits

Zinc oxide was obtained from SRL Chemical in Mumbai, Maharashtra, India. We procured low molecular weight chitosan (CS) with an average molecular weight of 50,000–190,000 Da, 75–85% deacetylation, and Dimethyl sulfoxide (DMSO), from Sigma Aldrich in Darmstadt, Germany. Ethanol, Ascorbic acid, penicillin, streptomycin, hydrocortisone, insulin, bovine serum, and Hematoxylin and eosin (H&E) were also sourced from SRL Chemical (Mumbai, Maharashtra, India). Purified water for the experiments was obtained from Milli-Q Type 1 Ultrapure Water Systems in Burlington, MA, USA. Ketamine was supplied by Boehringer Ingelheim in Germany. MEBO ointment from Golf Pharmaceutical Industrials in Ras Al-Khaimah, UAE, was purchased from the local market in Cairo, Egypt. Gentamycin ointment, TNF-α (tumor necrosis factor-alpha), IL-6 (Interleukin-6), IL-1β (interleukin-1 beta), IL-10 (Interleukin-10), and TNF-α (Tumor Necrosis Factor-alpha) human ELISA Kit were generously provided by Thermo Fisher Scientific (Life Technologies, CA, USA). Water used in the experiments was filtered using the Millipore MilliQ system. All other solvents and chemicals utilized were of analytical quality and used as provided.

## Plant Material and Extract Preparation

The Haraz Company, based in Cairo, Egypt, provided the authentically identified *Althaea Officinalis* (*A.O.*) F. Malvaceae flowers. To create water extract of *A.O.*, dried flowers weighing 1 kilogram were soaked in distilled hot water (60–70°C) for 4 hours within an aluminum foil-covered Erlenmeyer flask. The ratio of flowers to water used was 1:10. Afterward,

the extract was vacuum dried at 45°C using a rotary evaporator from Hei Dolph, Germany, after being filtered with Whatman filter paper no. 1. Then the extract was kept at 4°C until zinc oxide nanoparticles, or ZnO-NPs, turned green.[8,9]

## Phytochemical Screening of Active Constituents

To analyze the water flower extracts of *A.O*., a preliminary phytochemical screening was carried out using standard procedures. The objective was to qualitatively determine the presence or absence of various classes of phytochemicals in the extract, including phenolic compounds, flavonoids, mucilage, tannins, traces of saponins, polysaccharides, protein, and carbohydrates.[1,16]

## High-Performance Liquid Chromatography (HPLC-UV) Analysis of Phenolic Compounds in Althaea Officinalis (A.O)

In a research study, the extract of water flowers from *Althaea Officinalis* (*A.O*) was subjected to analysis using High-Performance Liquid Chromatography (HPLC). HPLC technique is widely used for the separation, identification, and quantification of various components present in a sample. We assessed the presence of major flavonoids and phenolic acids in *A.O*. against 17 phenolic standards. An Agilent 1260 series apparatus was used for the HPLC analysis, and a Zorbax Eclipse Plus C8 column with 4.6 mm x 250 mm dimensions and a 5µm particle size was used. Water (A) and a solution of 0.05% trifluoroacetic acid in acetonitrile (B) made up the mobile phase. A programmed linear gradient elution was used, with a constant flow rate of 0.9 mL/min. The gradient elution started at 82% A at 0 minutes, remained at that level for 1 minute, switched to 60% A for 18 minutes, and then returned to 82% A for the final 24 minutes. The wavelength at 280 nm was monitored using a multi-wavelength detector.[14,15] Each sample solution was injected into the system with a volume of 5µL. The temperature of the column was set at 40°C. Identification of phenolic compounds was achieved by comparing their retention times with those of standard compounds, as well as their corresponding UV spectra. The amounts of the compounds were calculated as milligrams for each gram of crude extract. The standard compounds that were used in this study to be phenolic and flavonoid were apigenin, benzoic acid, chlorogenic acid, cinnamic acid, ferulic acid, rutin, quercetin, and kaempferol.[9]

## Preparation of Althaea Officinalis -ZnO Nanoparticles

To synthesize zinc oxide nanoparticles using A.O. aqueous extract, we followed the following procedure: First, we added 40 mL of distilled water to a solution of zinc nitrate hexahydrate (0.1 M). Then, we added 20 mL of *A.O*. extract solution to the zinc nitrate solution and continuously stirred it at 150 °C for 2–3 hours until complete dissolution. The mixture was then allowed to cool to ambient temperature, and the supernatant was discarded. The resultant solid product was centrifuged twice at 6000 rpm for 10 minutes each time. It was a pale white color. Lastly, before being used in any research, the solid precipitate was dried for around eight hours at 60°C.[6,17]

## In vitro Characterization of A.O. -ZnO Nanoparticles (A.O.-ZnO-NPs)

### UV–Vis Spectroscopy Analysis

A Jasco V-630 spectrophotometer was used to measure the UV-Vis spectra of the ZnO-NPs and the *A.O*. aqueous extract at wavelengths ranging from 200 to 800 nm. The localized surface plasmon resonance (LSPR) spectra of ZnO-NPs were recorded using quartz crystal cuvettes with a scan speed of 200 nm/min and 2 mL of NPs in 1% sodium citrate.[1,17]

### Measurements of Particle Size and Zeta Potential

Using a Zetasizer Nano-Zs 90 instrument from Malvern International Ltd. in the UK, the particle size distribution, hydrodynamic diameter, and zeta potential were measured. We evaluated the dynamic size of the particles in the solution by monitoring the electrophoretic mobility of the samples and using dynamic light scattering (DLS) at a 90-degree scattering angle and a 25-degree Celsius temperature.[18,19]

## Morphology of A.O. -ZnO Nanoparticles Using Transmission Electron Microscope (TEM)

A transmission electron microscope (TEM) made by Tokyo, Japan-based JEOL, model JEM-1230, was used to visualize the morphology of the nanoparticles. 120 kilovolts (KV) was the acceleration voltage used for imaging. A carbon-covered copper grid was coated with diluted drops of the nanoparticle dispersion to obtain the optimal formulation for imaging. Subsequently,

the grid was dyed using a 1% phospho-tungstic acid solution and allowed to air dry for half an hour. The sample was then inspected under a microscope.[1,20]

## Fourier Transform Infrared Spectroscopy (FTIR)

FTIR analysis was carried out by mixing 5 mg of the sample with potassium bromide (100 mg) and pressed into disks using a hydraulic press. The resulting disks were then scanned using an FTIR spectrometer (model and make here) in the range of 400 to 4000 $cm^{-1}$. FTIR spectra obtained from the optimized *A.O.*-ZnO-NPs were compared to the corresponding plain ZnO nanoparticles to assess chemical compatibility between *A.O. A.O.* ZnO NPs.[18,21]

## Energy-Dispersive X-Ray (EDX) Spectrometry

The elemental composition of *A.O.* ZnO-NPs was assessed using EDX Spectrometry (JEOL model JSM-IT100, City and Country here. To perform this analysis, each element's unique peaks in the electromagnetic emission spectrum had to be examined.[1,6]

## Formulation and Characterization of CS Gel Containing A.O.-ZnO NPs

The right amount of CS was dissolved in a solution of 1% v/v aqueous acetic acid to create the CS solution (2% w/v). The mixture was stirred for 24 hours at room temperature, the solution was filtered with Whitman No. 1 filter paper. The filtrates were autoclaved for 15 minutes at 121 °C. To create the CS gel filled with *A.O.*-ZnO NPs[17,22]. This solution was then diluted with *Althaea Officinalis*-ZnO NPs produced through green synthesis, resulting in a 1% w/w CS gel. The mixture was shaken for 2 hours by adding 2 mL of glycerol were done using a magnetic stirrer. One milliliter of NaOH was added to the gel progressively until the pH reached 4.0. A placebo CS gel was made using the same methodology, excluding the addition of *A.O.*-ZnO NPs.

## Macroscopic Examination

We visually examined the color, homogeneity, consistency, and spreadability of the *A.O.*-ZnO-NPs CS gel formulation at the macroscale. Natural light was used to assess the clarity, and we made macroscopic measurements, comparing them to chitosan.[17,18]

## Accelerated Stability

*A.O.*-ZnO-NPs-containing CS gel stored at room temperature (20–25°C) to assess its conductivity, pH, viscosity, color, and odor. Furthermore, by subjecting the *A.O.*-ZnO-NPs CS gel to temperatures ranging from 4°C to 40°C for 12 days, the gel's resilience to freeze-thaw cycles was investigated. Eight months after the formulation was developed, the tests were carried out, with each test being run in triplicate using 30-gram samples.[18,19]

## Centrifugation Test

To perform the centrifugation test, 10 grams of the formulation were placed in a tapered test tube. The test tube was then subjected to centrifugation for 30 minutes at room temperature using a cycle of 3000 rpm. The centrifugation was carried out using equipment from the Ajanta Doctor Model.[23]

## Spreadability Test

To assess the spreadability of the *A.O.*-ZnO-NPs CS gel, a method involving glass plates was employed. A glass plate with a diameter of 2 cm was marked with a circle, and 0.5 g of the formulated CS gel was applied within the marked area. Another glass plate was then placed on top. After allowing a half kilogram of weight to rest on the upper glass plate for five minutes, the gel was left to spread. The diameter of the gel spread within the circle was measured.[18,22]

## Conductivity and pH Tests

*A.O.*-ZnO-NPs CS gel formulation's pH and conductivity were assessed using a digital pH meter (WTW portable PH meter model 3110 Germany). The conductivity was measured in millivolts (mV). For the preparation to reach

equilibrium while being measured, it was left alone for around 15 minutes. The pH of each formulation and conductivity were measured in triplicates, and average values were computed.[8,23]

## Viscosity Test

A viscometer (Quimis® MOD 0860M21) was used to test the viscosity of the *A.O.*-ZnO-NPs CS gel. 10, 20, 30, 40, 50, and 60 rotations per minute were applied to the gel. The relevant dial reading was recorded for each speed.[18,22]

## Antioxidant Activity Assay

For forty minutes, two mL of the *A.O.*-ZnO-NPs chitosan solution and two mL of the 0.1 mM DPPH solution were combined in methanol.[1,24] For testing antioxidant activity, Ascorbic acid (50 mg/20 mL MeOH, 0.008 mol) was utilized as a positive control sample. The absorbance was measured using spectrophotometry at (200–800 nm), with methanol serving as a blank.[8,18] The mixture was combined and swirled at 25 C for 45 minutes in a glass bottle with an amber hue. The produced violet color absorbance was measured at (200–800 nm), using spectrophotometry, and the following relation was used to determine the percentage of antioxidant activity:

$$\%\frac{\text{Antioxidant 1}}{\text{Antioxidant 2}}\times \text{ radical scaenging assa} = \frac{(\text{A0}-\text{A1})}{\text{A0}}\times 100$$

where A0 is the blank absorbance sample, and A1 is the absorbance of A.O.-ZnO-NPs chitosan.

## Antimicrobial Analysis

To evaluate the antibacterial activity of the formulated CS gel, we explored the inhibition or clearance zone's diameter against *Staphylococcus aureus, Bacillus subtilis* (Gram-positive) and *Escherichia coli, Pseudomonas aeruginosa* (Gram-negative) in seeded agar plates. Samples of *A.O* aqueous extract, *A.O*-ZnO-NPs, *A.O*-ZnO-NPs CS gel, and the standard agent Gentamicin were evaluated. Al-Azhar University Regional Center for Mycology and Biotechnology provided us with standardized bacterial strains. The diffusion agar technique was used to measure the antibacterial activity. Nutrient agar medium was poured into Petri plates, and wells were created using a sterile cork borer.[2,25] A sterile cork borer loaded with predetermined amounts of ZnO-NPs, *A.O.* aqueous extract, and *A.O.*-ZnO-NPs CS gel (100µg) was used to introduce the samples into the wells. After that, the Petri plates were incubated for 24 hours at 37°C. Using a ruler, the diameter of the inhibition zone encircling each well was measured, and the average diameter was determined. The inhibition zones' mean and standard deviation (SD) for each tested material were determined from six samples. A positive control of 4 µg/mL was employed with Gentamicin. We used the broth microdilution method in 96-well plates to find the minimum inhibitory concentration (MIC). In 96 wells, we serially diluted 200µg/mL of *A.O.* aqueous extract, *A.O.*-ZnO-NPs, and *A.O*-ZnO-NPs CS gel. Next, 100 µL of standardized various bacterial strains.[18]

## In-Silico Molecular Modeling Study

The open-source software, Auto Dock Vina v1.1.2.[26,27] was used for carrying out the docking study. The 3D protein structures were downloaded from the protein data bank.[27] (https://www.rcsb.org/) as pdb format for tumor necrosis factor-alpha "TNF-α" (ID: 2AZ5), interleukin-1β "IL-1β" (ID: 6Y8M), glycogen synthase kinase 3-β "GSK3-β" (ID: 3F88), matrix metalloproteinases-8 "MMP-8" (ID: 5H8X) and nitric oxide synthase "iNOS" (ID: 3N2R). Protein and ligand preparations were performed by MGL tools 1.5.7. and both files were saved as pdbqt which is the required format needed in Auto Dock Vina docking procedure. The protein-ligand interaction patterns were visualized by the BIOVIA Discovery Studio Visualizer v21.1.0.20298.[27]

## Cell Culture Assays, Determination of Proinflammatory Cytokine

### Cytotoxicity Assays

Human Skin Keratinocyte (Hacat) cells were purchased commercially from American Type Culture Collection ATCC Manassas, VA, USA),(ATCC PCS-201–012) via VACSERA Egypt for in vitro cytotoxicity assessments to evaluate the impact of these formulations on the skin. These cells were cultivated in serum-free keratinocyte media in the presence of

various substances. The media included 100 ng/mL of penicillin, 100 mg/mL of streptomycin, 500 ng/mL of hydrocortisone, 0.005 mg/mL of insulin, and 10% bovine serum. Additionally, the solution was supplemented with 0.005 mg/mL of bovine pituitary extract and 5 ng/mL of epidermal growth factor to the final concentration.[18,19]

To ensure optimal growth, the HaCat cells were cultured in a flask under specific conditions until they reached approximately 80% confluence.[28] These conditions included a controlled 37°C temperature and a humidified environment with 10% $CO_2$ concentration. MTT assay (3-(4,5-dimethyl-2-thiazolyl)-2,5-diphenyltetrazole bromide) was used as a measure of cell viability. After incubating the cells for 24 hours at 37°C, they were transferred to a 96-well plate. Subsequently, the cells were exposed to varying concentrations (ranging from 0.05 to 0.1 mg/mL) of *A.O.* aqueous extract, *A.O.*-ZnO-NPs, and *A.O.*-ZnO-NPs-Cs in a new medium for two hours. Following exposure, the cells were treated with a 0.25% MTT solution and incubated for an additional 24 hours. The cells were then treated further after being cleaned with phosphate-buffered saline (PBS). After the media was removed, the cells were lysed using dimethyl sulfoxide (DMSO). The Modulus™ microplate reader, manufactured in California, USA by Turner BioSystems, was utilized to measure absorbance at 560 nm. The results of the MTT assay were expressed as the proportion of cells that exhibited reduced viability compared to the untreated (control) cells.[5,14]

## Assessing the Immune Response of Cytokine Production Serum Level

Three hours after administering lipopolysaccharide (LPS) to rats, blood samples were collected from the tail vein.[29] The levels of inflammatory cytokines, including interleukin (IL)-6, anti-inflammatory cytokine IL-10, interleukin (IL)-1β, and tumor necrosis factor (TNF-α), in the serum were evaluated using commercially available cytokine ELISA kits from Excell, headquartered in Shanghai, China. The measurements were conducted by the operating procedures outlined in the ELISA kit for the cytokine enzyme-linked immunosorbent assay.[22,30]

## In vivo Study

### Experimental Design

An excision wound model in adult male Albino Wistar rats was used to assess the efficacy of the prepared formulations. Forty mature male albino rats, weighing between 180 and 200 G that are 8 and 12 weeks old, were obtained from the Alexandria University animal house located faculty of medicine in Alexandria, Egypt. For a week, they were acclimated to regular environmental circumstances, which included a natural light/dark cycle, a consistent temperature of 22–25 °C, and a relative humidity of 45–60%. Throughout the study, the rats were given unlimited access to water and regular pellet meals in wire mesh cages made of plastic. All protocols and care procedures for the animals were performed by the Animal Ethics Committee rules at Alexandria University Faculty of Medicine in Alexandria, Egypt (Approval 0306487). Ketamine was used to induce anesthesia in the animals at 80 mg/kg dose.[31] The rats' dorsal fur was meticulously shaved using an electric clipper, and each animal's dorsal side was marked with the location of the wound. In each rat, a 4 cm in length and 2 mm in depth excision was made. The rats were then randomly divided into five groups, with eight rats in each group. Group 1's wounds were left untreated, but group 2's wounds received normal medication (mobo and gentamycin). In group 3, an extract from *A.O.* was used to heal the wounds. ZnO-NPs were used to treat the wounds in group 4, and a combination of *A.O.* and ZnO-NPs CS gels were used to treat the wounds in group 5. For 14 days, the treatments were applied topically to the corresponding groups every other day.[32,33]

## Percentage of Wound Contraction

Wound healing is a complex process that involves the restoration of damaged skin to its original state. During this process, wound contraction plays a significant role in reducing the size of the wound. To assess the progress of wound closure at different treatment stages, the wound area is measured. Wound contraction refers to the gradual changes in the size of the wound and is often expressed as the percentage reduction in the original wound size 37. To calculate the wound contraction percentage, the equation used is:

$$\text{Wound contraction percentage} = 1-(\text{Ad}/\text{A0})\times 100$$

Here, A0 represents the wound area on day zero (the initial measurement), and Ad represents the wound area on the corresponding day being evaluated. By calculating the reduction in wound size, we can track the progress of wound closure over time.

## Histopathological Studies

To evaluate the progress of wound healing, skin tissue samples were obtained from the wound site on the 3rd, 7th, and 14th days and underwent histopathological examinations. Biopsy specimens were meticulously preserved in a 10% buffered formalin solution and forwarded to the pathology lab for hematoxylin and eosin staining to study the histology.[34]

## Statistical Analysis

The in vitro data was provided as mean ± SD. In contrast, in vivo data were presented as mean ± SEM or median and interquartile change. The differences between groups were analyzed using mean values together with matching standard deviations (SD). Using the SPSS Statistics program (version 16), the one-way analysis of variance (ANOVA) approach was used to do the statistical analysis of the data. When a p-value was ≤0.05, it was deemed statistically significant and Tukey's post-hoc test for multiple comparisons. Non-parametric score data was analyzed using Kruskal–Wallis and Dunn multiple comparison tests. The findings were statistically analyzed using Graph Pad Prism 8.0.2 (La Jolla, CA, USA).

# Results and Discussion

## Phytochemical Analysis of the Althaea Officinalis (A.O.) Flowers Aqueous Extract

Initial phytochemical screening of water-based extract of *Althaea Officinalis* (*A.O.*) flowers was positive for, flavonoids, mucilage, phenolic, polysaccharides, and traces of saponins, Preliminary phytochemical analysis was shown (Table 1).

## (HPLC) Analysis for Identification of Components Present in the Aqueous Extract

The phenolic components of the *A.O.* flower's aqueous extract were identified and quantified through HPLC analysis, with eighteen peaks being detected at 248 nm under optimal conditions as shown in Figure 1 and Table 2. Among these peaks, Phenolic acids: Gallic acid, Chlorogenic acid, Methyl gall, Caffeic acid, Syringic acid, Pyrocatechol, Ellagic acid, Coumaric acid, Vanillin, Ferulic acid, Rosmarinic acid, Quercetin, Cinnamic acid, and Kaferol were identified and quantified as major constituents. Among these peaks, are flavonoids: Naringenin, Daidzein, Quercetin, Kaempferol, and Hesperetin.[7,9]

Gallic acid was found to be the most abundant phenolic compound in the *A.O.* aqueous flower extract, with a concentration of 29.65 µg/mL. The most abundant flavonoid compounds in 50.93 µg/mL were found to be Quercetin.

**Table 1** Initial Phytochemical Screening of Water-Based Extract of Althaea officinalis (A.O) Flowers

| No. | Phytochemical test | *Althaea officinalis* flowers |
|---|---|---|
| a | Test for Flavonoids (NaOH/HCL test) | ++ ve |
| b | Test for Saponins (Froth test) | + ve |
| c | Test for Mucilage (Ruthenium test) | + ve |
| d | Test for Tannins ($FeCl_3$ test) | + e |
| e | Test for Carbohydrates (Molisch test) | + ve |
| f | Test for Cardiac Glycosides (Keller–Killiani test) | - ve |
| g | Test for phenolic (Millon's test) | ++ ve |
| H | Test for polysaccharides (Iodine Test) | + ve |

**Notes**: (++ ve) indicates a high presence of constituents, (+ ve) indicates a mild presence of constituents, and (– ve) indicates absence of constituents.

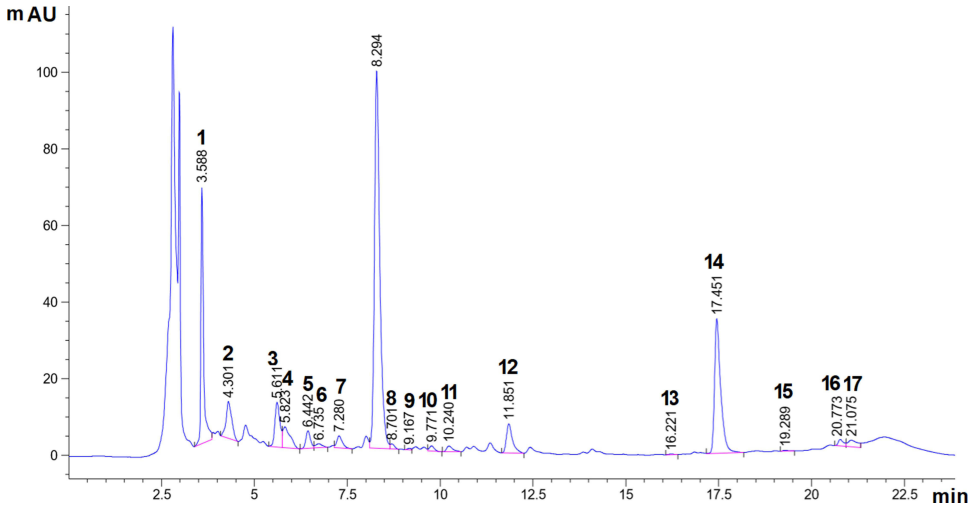


**Figure 1** HPLC chromatograms of the marshmallow aqueous flower extract includes both phenolic acids and flavonoids.

## In vitro Characterization of Althaea Officinalis -ZnO Nanoparticles (A.O.-ZnO NPs)

### UV-Vis Spectroscopic Analysis

The UV-Vis spectral analysis is depicted in Figure 2A illustrates the findings from the examination of the *A.O.* flower aqueous extract and the synthesized ZnO nanoparticles (NPs). The generation of ZnO NPs was investigated using a UV-Vis spectrophotometer, specifically focusing on the surface plasmon resonance (SPR) at 390 nm. This SPR peak is indicative of the intrinsic bandgap of ZnO, representing the electron transition from the valence band to the conduction band (Zn 3d——O2p).In the UV-Vis analysis of the *A.O.* flower aqueous extract, an absorption band at 245 nm was observed, corresponding to the π*–π* transition,[1,6] suggesting the presence of phenolic components in the extract. However, this absorption band is no longer evident in the synthesized ZnO-NPs, indicating the active involvement of the phytochemicals present in the *A.O.* aqueous extract in the formation of the nanoparticles.

**Table 2** Compound, Retention Times, and Area Peaks of Althaea Officinalis Flowers Extract in Water

| Peak No. | Compounds | Retention Time | Area % | Conc (µg/mL) |
|---|---|---|---|---|
| 1 | Gallic acid | 3.59 | 25.83 | 296.50 |
| 2 | Chlorogenic acid | 4.30 | 7.85 | 137.78 |
| 3 | Methyl gallate | 5.61 | 8.43 | 56.64 |
| 4 | Caffeic acid | 5.82 | 5.84 | 61.94 |
| 5 | Syringic acid | 6.44 | 3.06 | 29.75 |
| 6 | Pyro catechol | 6.735 | 1.06 | 20.06 |
| 7 | Rutin | 7.12 | 0.26 | 5.31 |
| 8 | Ellagic acid | 7.28 | 0.80 | 29.71 |
| 9 | Coumaric acid | 8.70 | 0.80 | 3.84 |
| 10 | Vanillin | 9.17 | 0.24 | 1.17 |
| 11 | Ferulic acid | 9.77 | 1.01 | 7.92 |
| 12 | Naringenin | 10.24 | 1.33 | 16.45 |
| 13 | Rosmarinic acid | 11.85 | 6.61 | 93.85 |
| 14 | Daidzein | 16.22 | 0.12 | 0.89 |
| 15 | Quercetin | 17.45 | 31.00 | 509.28 |
| 16 | Cinnamic acid | 19.29 | 0.21 | 0.49 |
| 17 | Kaempferol | 20.77 | 1.32 | 11.25 |
| 18 | Hesperetin | 21.08 | 2.47 | 16.50 |

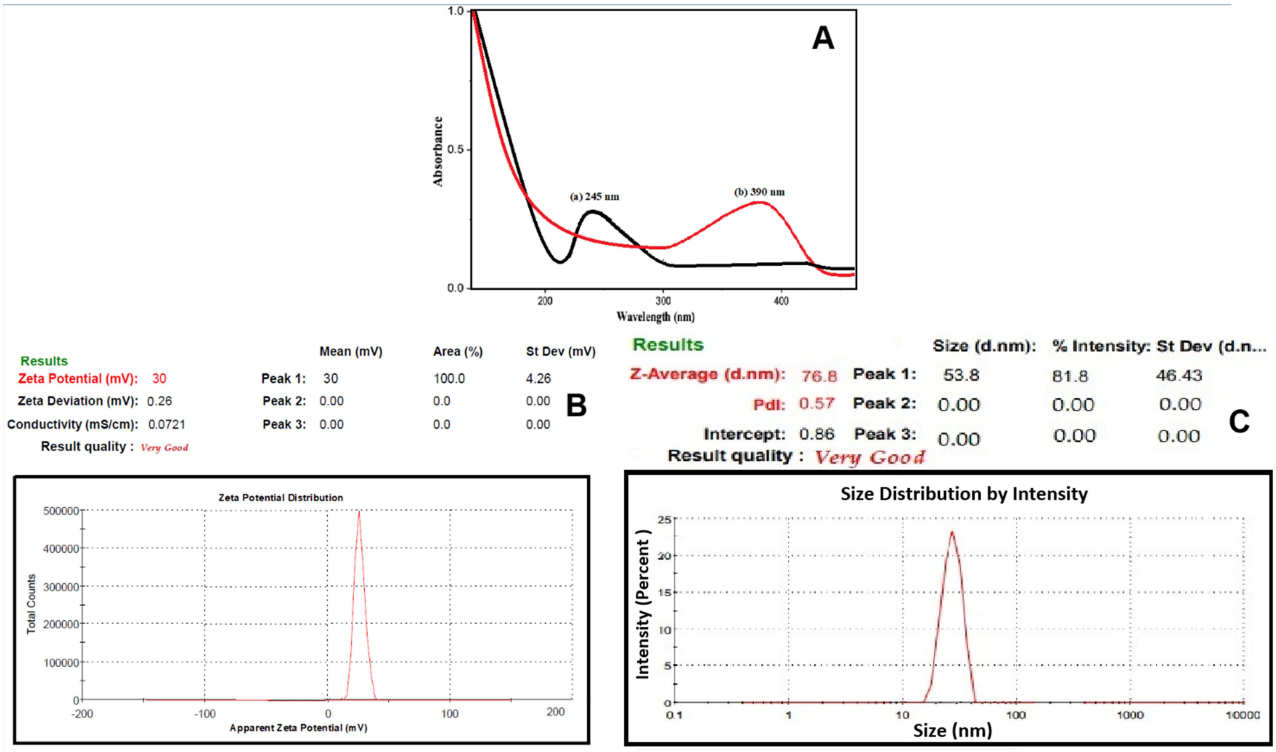


**Figure 2** (**A**) UV-Vis absorption spectra of (a) *althaea officinalis* extract and (b) Green ZnO nanoparticles and (**B**) Determination of zeta potential (**C**) and size of green Zno-NPs by DLS measurement.

## Measurements of Particle Size and Zeta Potential

Using the Dynamic Light Scattering (DLS) method, the Zeta potential of these nanoparticles was measured to be +30 mV. This finding suggests that the active compounds present in the plant extract interacted with the surface of the ZnO-NPs, leading to their stabilization. Our study also demonstrated that the ZnO-NPs possessed a positive charge of +30 mV (as depicted in Figure 2B). A zeta potential equal to or greater than +30 mV indicates the dispersion of NPs in a stable manner, Additionally, the particle size of biosynthesized ZnO-NPs was approximately 76 nm (as depicted in Figure 2C). These outcomes confirm that the active compounds found in the *A.O.* aqueous extracts, such as phenolic acids and flavonoids, likely contributed to the positive zeta potential, consequently enhancing the stability of the NPs. The positive zeta potential generates repulsive forces within the colloidal solution of ZnO-NPs, preventing their aggregation.[6,14]

## Transmission Electron Microscopy (TEM) Analyses

The predominant morphology of the particles shown in Figure 3A was spherical, although some triangular, hexagonal, and rod-like shapes were also present. This can be attributed to the influence of biomolecules, particularly flavonoid glycosides, phenolic acids, tannins, and flavonoids, which play a role in directing the growth of various shapes during biomineralization. When examined using transmission electron microscopy (TEM), the ZnO-NPs appeared predominantly spherical, with particle sizes ranging from 50 to 70 nm.[19,35]

## Fourier Transform Infrared (FTIR) Spectroscopy Analysis

The FTIR spectrum of ZnO nanorods synthesized using an *A.O.* extract was analyzed and is presented in Figure 3B. This spectrum displayed characteristic bands at specific wavenumbers, including 3370 $cm^{-1}$, 2966 $cm^{-1}$, 1640 $cm^{-1}$, 1397 $cm^{-1}$, 1016 $cm^{-1}$, and 580 $cm^{-1}$. The purpose of utilizing FTIR spectroscopy was to investigate the potential functional groups of phytochemicals present in the *A.O.* extract that may be responsible for reducing $Zn(NO_3)_2$. Several notable absorption peaks were observed in the spectrum, including a strong peak at 3326 $cm^{-1}$ corresponding to the stretching vibrations of -OH groups and aliphatic methylene groups (-C-H stretching). The most prominent band at

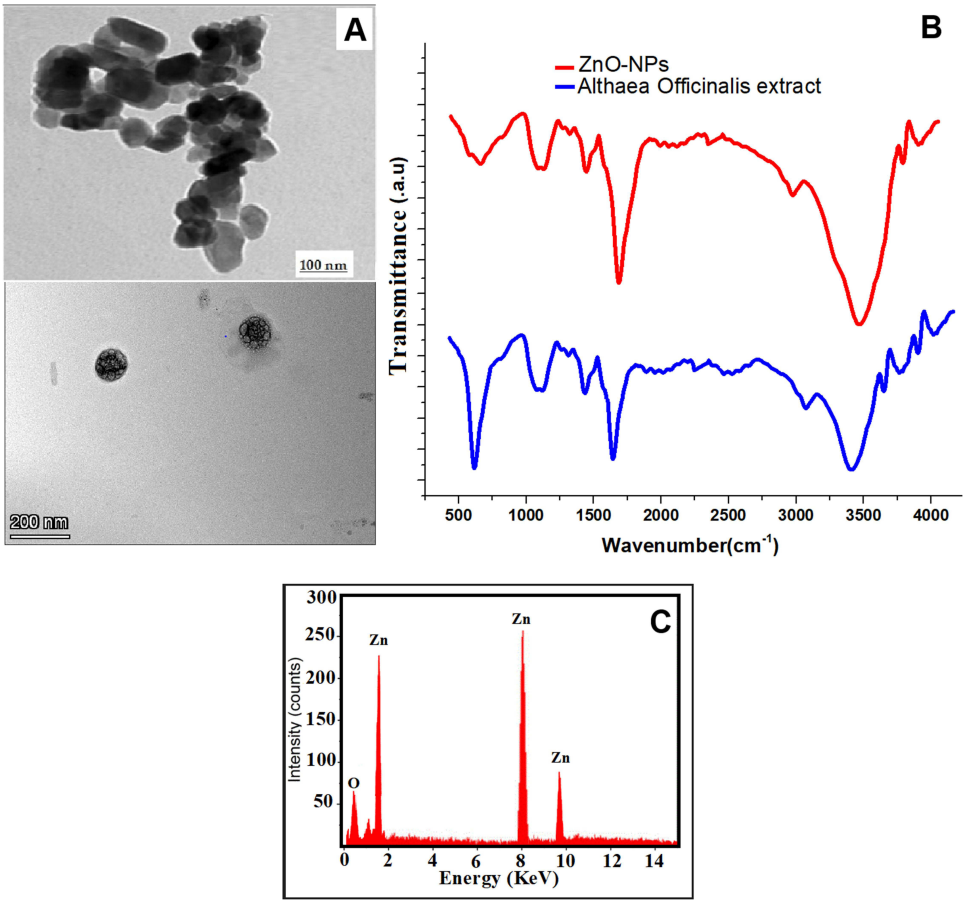


**Figure 3** (**A**) Determination of size and shape of green ZnO-NPs by TEM (**B**) FTIR spectra of the biosynthesized ZnO nanoparticles using *Althaea Officinalis* extract and (**C**) EDX of Zinc Oxide nanoparticles made by *Althaea Officinalis*.

1635 $cm^{-1}$ represents vibrations related to C=O bonds, typically found in the structure of flavonoids present in the A. officinalis extract. Furthermore, the absorption band at 1348 $cm^{-1}$ can be attributed to the bending vibrations of the CH groups in the aromatic tertiary amine. The spectrum also displayed bands at 403 $cm^{-1}$ and 424 $cm^{-1}$, indicating metal-oxygen stretching related to the ZnO nanostructure formation. These findings further support the presence of active compounds within the *A.O*. aqueous extract.[6,30]

## Energy-Dispersive X-Ray Spectroscopy

The EDX analysis, showcased in Figure 3C, was conducted to quantitatively assess the elemental composition of ZnO NPs synthesized using green methods. The "EDX spectrum" of ZnO NPs exhibited two major peaks: zinc at 2.8 keV and oxygen at 0.5 keV, indicating the biogenic fabrication of ZnO NPs. The EDX analysis of ZnO NPs synthesized by *A.O*. determined the elemental formulation and the mass percentages of zinc and oxygen, which were found to be 80.3% and 19.7%, respectively, as illustrated in Figure 3C. Remarkably, our study's EDX analysis yielded similar results for both synthesized nanoparticles. It is noteworthy to mention that a previous study reported elemental composition values of approximately 15.02% for zinc and 7.21% for oxygen, which could be attributed to the presence of various phytochemicals in the *A.O* extract.[1,6]

## Characterization of Chitosan (CS) Gel Containing ZnO- NPs

The macroscopic properties and attributes of the *A.O*. ZnO- CS gel formulation, such as color, aspect, transparency, homogeneity, Spreadability, and scent, were evaluated. The (*A.O*.-ZnO-NPs) gel formulation has a uniform white hue, a smooth texture, and a distinctive aroma of *A.O*. aqueous extract. Eight months after development, the (*A.O*.-ZnO-NPs) features remained the same, and there was no difference between the aspects of (*A.O*.-ZnO-NPs) before and after a

**Table 3** Physical Characterization of CS Gel and CS Gel Containing ZnO-NPs and Evaluation of the Preliminary Stability of AO-ZnO-NPs Before and After the Freeze-Thaw Cycle

| Formulation | Appearance | Ph | Spreadability ($Cm^2$) | Viscosity (cps) | Conductivity | Centrifugation |
|---|---|---|---|---|---|---|
| **CS gel(placebo)** | Homogeneous, transparent, Colorless | 3.84±0.01 | 53.11±0.24 | 601.01±0.22 | 192.02±0.15 | No noticeable instability in the formulation. |
| ***AO*-ZnO NPs CS gel (before)** | Homogeneous, transparent, Colorless | 4.21±0.21 | 56.31±0.37 | 603.13±0.35 | 190.04±0.33 | No noticeable instability in the formulation. |
| ***AO*-ZnO NPs CS gel (After)** | Homogeneous, transparent, Colorless | 3.91±0.32 | 52.91±0.45 | 601.02±0.41 | 189.04±0.25 | No noticeable instability in the formulation. |

freeze-thaw cycle. CS was employed in our study to create a gel matrix and evenly disperse *A.O*. ZnO-NPs within it. It has been widely established that chitosan gel is biocompatible and has desirable safety properties for live tissues.[18,36] Additionally, several studies have shown that CS is a highly effective antibacterial agent that may stop the development of a variety of microorganisms, including bacteria and fungi. Because it is hydrophilic, chitosan may hold onto water inside of its structure and CS gel at acidic pH levels. CS gel was created at a 2% w/v concentration due to its desirable spreadability and consistency, as shown in (Table 3).

The gel created from *A.O*.-ZnO-NPs exhibited stable pH values and conductivity, with no significant differences observed between conductivity measurements before and after the freezing-thawing cycle. This suggests that the gel can be utilized topically without any concerns. Table 3 presents the physical and chemical characteristics of A.O.-ZnO-NPs before and after a twelve-day freeze-thaw cycle. *A.O*.-ZnO NPs CS gel was found to have a narrow time spread, indicating its high spreadability.[37] The distribution of gels plays a role in their therapeutic effectiveness, and manufactured gels need to have optimal spreadability for uniform application on the skin. This factor also contributes to patient adherence to therapy. The consistency of the CS gel is crucial for topical antimicrobial and anti-inflammatory formulations as they are applied to thin layers of the skin.[22,36] The viscosity of the gel plays a vital role in controlling the medication's permeation. Figure 4 shows the behavior of chitosan and *A.O*.-ZnO-NPs during six different viscosity tests at various rotational speeds (10, 20, 30, 40, 50, and 60 rpm).

## Antioxidant Activity Assay

The human body's natural defense against free radicals, known as antioxidants, can be overwhelmed, leading to the oxidation of proteins and fats, and causing oxidative stress, a factor in degenerative diseases. Medicinal plants provide

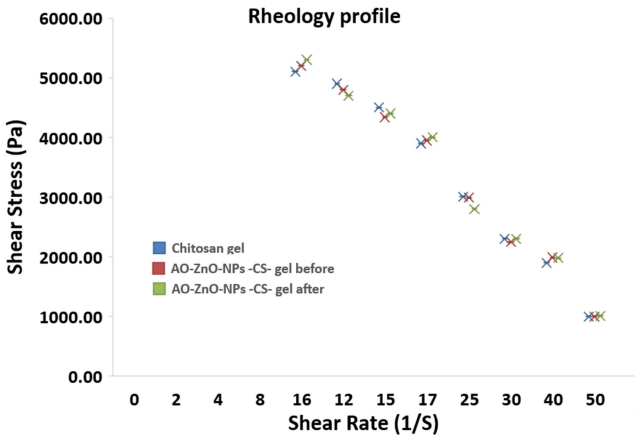


**Figure 4** The rheological profile of Chitosan gel and Chitosan gel containing *Althae Officinalis* ZnO NPs before and after the freeze-thaw cycle exhibited pseudoplastic behavior.

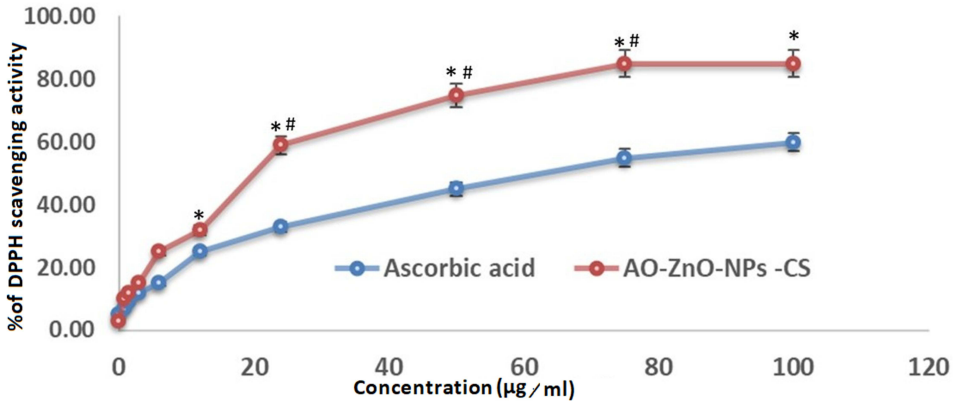


**Figure 5** The oxidative properties of Ascorbic Acid and *A.O.* Zn-NPs-Cs against DPPH. The data are presented as means ± SE (n = 6). Significance *Relative to the Ascorbic Acid, #Relative to the previous concentration.

valuable sources of antioxidants to maintain overall health. In this study, the antioxidant activity of *A.O.*-Zn-NPs-Cs was assessed using DPPH, a stable free radical that changes color from purple to yellow in the presence of antioxidants. Antioxidants scavenge the DPPH radical by donating hydrogen radicals (H•), resulting in the formation of stable DPPH-H molecules. As shown in Figure 5, the radical scavenging activity of ascorbic acid and nanoparticles increased with higher concentrations. The IC50 values, which represent the concentration required to scavenge 50% of the DPPH radical, were found to be 4.23 ± 0.12 µg/mL for *A.O.*-Zn-NPs-Cs and 11.96 ± 0.32 µg/mL for ascorbic acid, as shown in Table 4. These results demonstrate that the nanoparticles possess potent antioxidant potential, surpassing that of the ascorbic acid standard, and are consistent with previous studies. The antioxidant activity of the nanoparticles can be attributed to the presence of various phytochemicals, which likely work synergistically to combat free radicals.[1,38] These findings strongly support the use of *A.O.*-mediated Zn-NPs derived from flower extracts as natural antioxidants, offering protection against oxidative stress associated with degenerative diseases.

## Antibacterial Activity of ZnO NPs

*Staphylococcus aureus, Bacillus subtilis* (Gram-positive) and *Escherichia coli, Pseudomonas aeruginosa* (Gram-negative) were used to assess the bactericidal effects of *A.O.*-ZnO-NPs-CS gel, *A.O.*-ZnO-NPs, and *A.O.* aqueous *extract*. Zones of inhibition of *S. aureus and Pseudomonas aeruginosa* against common medications Gentamycin at concentrations ranging from 4 µg/mL (100 µL). Three replicates' average zone of inhibition (mm) values. Standard Gentamycin and biosynthesized NPs were evaluated, and the results showed a stronger antibacterial. Standard medicines' zones of inhibition in *Staphylococcus aureus, and Bacillus subtilis* were resistant to several common medications, and the zone of inhibition for the remaining common medications was 20.00mm, whereas those of AO-ZnO-NPs-CS gel was 19.04 mm, whereas those of AO-ZnO-NPs were 15.01 mm and 13.01 for *A.O.* aqueous extract. Zones of inhibition and standard medication potency according to WHO guidelines are shown in (Table 5). *S. aureus* exhibited a minimum inhibitory concentration (MIC) of 6 µL when exposed to the chitosan gel containing ZnO-NPs.[2,6] As the concentration of CS-NPs increased, the zone of inhibition also increased. Statistical data clearly show that the zone of inhibition for *A.O.* -ZnO- CS NPs was significantly larger against *S. aureus* and *Bacillus subtilis* compared to *Escherichia coli, and Pseudomonas aeruginosa* (Figure 6). The relatively weaker

**Table 4** The $IC_{50}$ of A.O.-ZnO-NPs-Cs and Ascorbic Acid in the DPPH Test

| | A.O.-ZnO-NPs-Cs | Ascorbic Acid |
|---|---|---|
| $IC_{50}$ of DPPH | 4.23 ± 0.12 µg | 11.96 ± 0.32 µg |

**Notes**: IC50 is the concentration of NPs that can scavenge DPPH radicals by 50%.

**Table 5** In-Vitro Anti-Microbial Susceptibility of Althea Officinalis (A.O) Extract, A.O-ZnO-Nps, Chitosan (CS) Gel of A.O.-ZnO-NPs, and Gentamycin (Control) (n = 3 ± SD)

| Bacterial Strains | Item Under Test | Diameter of Zone in (mm) (Mean± SD) | MIC (µg/mL) (Mean ± SD) |
|---|---|---|---|
| ***Staphylococcus aureus*** **(ATCC 25923)** | **Chitosan gel of *A.O*-ZnO-NPs** | 19.04 ± 0.42 | 16.54 ± 0.42 |
| | ***Althea Officinalis* (*A.O*) extract** | 13.01±0.13 | 27.84±0.24 |
| | ***A.O*-ZnO-Nps** | 15.01 ± 0.11 | 20.74 ± 0.25 |
| | **Gentamycin** | 20.0.00± 0.23 | 17.21 ± 0.51 |
| ***Bacillus subtilis*** **RCMB 015 (1) NRRL B-543** | **Chitosan gel of *A.O*-ZnO-NPs** | 22.51 ± 0.22 | 18.41 ± 0.35 |
| | ***Althea Officinalis* (*A.O*) extract** | 15.52±0.24 | 29.14±0.51 |
| | ***A.O*-ZnO-Nps** | 18.01 ± 0.33 | 22.01 ± 0.55 |
| | **Gentamycin** | 22.0.21± 0.25 | 18.33 ± 0.35 |
| ***Escherichia coli*** **(ATCC 27853)** | **Chitosan gel of *A.O*-ZnO-NPs** | 20.11 ± 0.15 | 17.04 ± 0.22 |
| | ***Althea Officinalis* (*A.O*) extract** | 14.51±0.51 | 24.12±0.41 |
| | ***A.O*-ZnO-Nps** | 17.02 ± 0.31 | 19.04 ± 0.15 |
| | **Gentamycin** | 26.021± 0.51 | 18.51 ± 0.35 |
| ***Pseudomonas aeruginosa*** **(ATCC 27853)** | **Chitosan gel of *A.O*-ZnO-NPs** | 9.51 ± 0.32 | 30.01 ± 0.11 |
| | ***Althea Officinalis* (*A.O*) extract** | NA | NA |
| | ***A.O*-ZnO-Nps** | NA | NA |
| | **Gentamycin** | 19.01 ± 0.13 | 20.0 ± 0.23 |

inhibitory effect of *A.O*. ZnO- CS-NPs on *Escherichia coli, Pseudomonas aeruginosa*, when compared to *Staphylococcus aureus, Bacillus subtilis*, can be attributed to differences in the membrane structure of Gram-positive and Gram-negative bacteria.[39] Gram-positive bacteria have a thicker cell wall due to the presence of a peptidoglycan layer. It has been reported that the combination of ZnO-NPs with chitosan can cause damage to bacterial cell membranes, leading to the leakage of intracellular contents and ultimately resulting in bacterial cell death. Tables 5 and Figure 6 show that A.O. ZnO- CS-NPs inhibited Gram-negative and Gram-positive bacteria better than chitosan or zinc oxide alone. Three proposed chitosan action mechanisms for microbial inhibition have been reported. Polycationic chitosan chains interact electrostatically with the polyanionic bacterial cell membrane, according to the most plausible theory. This changes its permeability and leaks electrolytes and proteins. Increased cationic sites on the antimicrobial drug boost inhibition, according to this theory. Since they are easily protonated, the extra polar groups improve the hydrophilicity, swelling ability, and number of cationized sites of A.O. ZnO- CS-NPs and CS. This boosts their positive charge strength, electrostatic contact with microbial cell membranes, and antibacterial activity.[40] The third approach used chitosan's strong binding effects on spore elements, metals, and critical nutrients. It is widely known that imine and/or hydrazide compounds chelate metals.[17] The addition of hydrazide linkages, imine moieties, and regained amino groups to of A.O. ZnO- CS-NPs and CS increases the number of chelating sites for spore elements, metals, and essential nutrients, making these zinc oxide nanoparticles loading with chitosan more potent against bacteria than chitosan alone.

## In-Silico Study

*Althaea officinalis* identified major components that were docked into five of the most important protein targets that play an important role in wound healing mechanisms which are TNF-α, IL-1β, GSK3-β, MMP-8, and iNOS.[41,42] The five

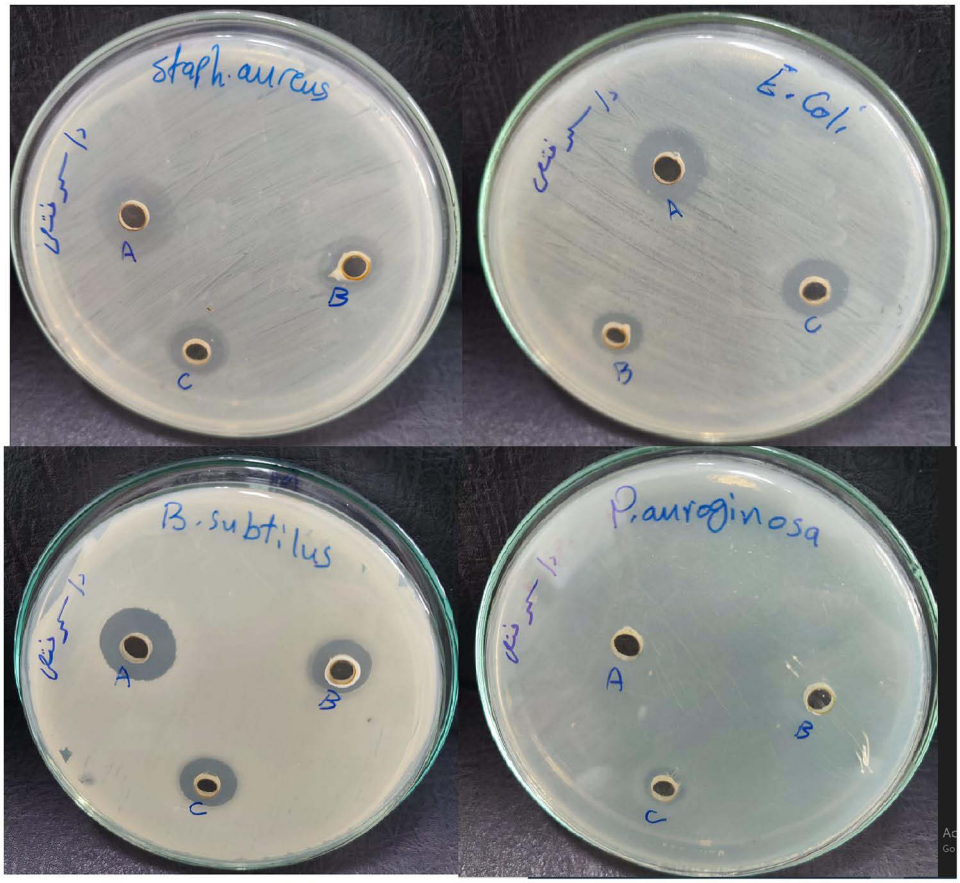


**Figure 6** In-vitro Antibacterial study for chitosan gel of *A.O*-ZnO-NPs (A), *Althaea Officinalis* extract (B), and *A.O*-ZnO-NPs (C) using agar cup diffusion method.

tested components are quercetin, gallic acid, methyl gallate, chlorogenic acid, and rosmarinic acid (Figure 7). The docking energy scores in kcal/mol. of the tested components against the co-crystallized ligand in each of the five protein files are listed in Table 6.

Quercetin, chlorogenic acid, and rosmarinic acid exhibited the highest binding energy scores for all the tested targets revealing their predicted great role in wound healing mechanisms. For TNF-α, the binding score for the three derivatives are −10.2, −8.6, and −9.8 kcal/mol., respectively. They showed the key interactions with GLY121 through hydrogen

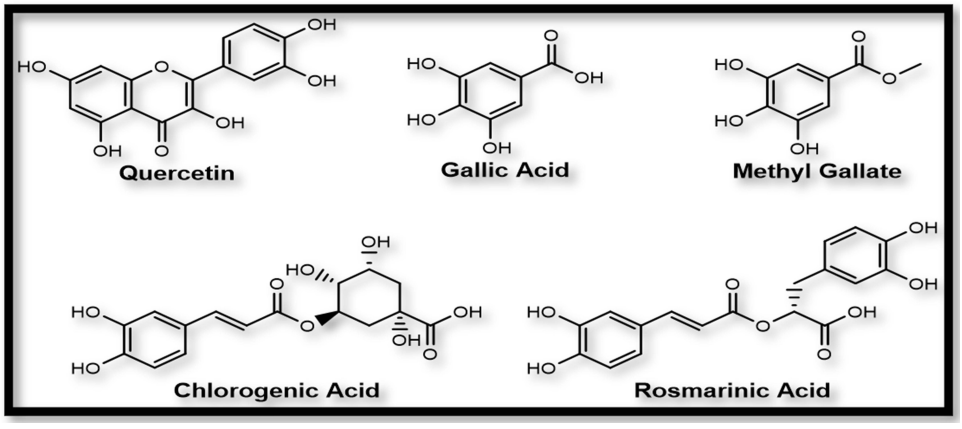


**Figure 7** Structures of the major identified components of *Althaea officinalis* extract.

**Table 6** The Docking Energy Binding Scores in kcal/mol. for the Tested Compounds

| | TNF-α | IL-1β | GSK3-β | MMP-8 | Inos |
|---|---|---|---|---|---|
| **Co-crystallized ligand** | −9.7 | −7.7 | −9.9 | −9.8 | −10.1 |
| **Quercetin** | −10.2 | −7.8 | −9.6 | −11.6 | −10.9 |
| **Gallic acid** | −5.7 | −7.1 | −6.1 | −8.6 | −10.1 |
| **Methyl gallate** | −6.2 | −7.7 | −6.6 | −9.0 | −9.2 |
| **Chlorogenic acid** | −8.6 | −9.4 | −11.1 | −12.2 | −11.0 |
| **Rosmarinic acid** | −9.8 | −9.2 | −11.3 | −11.6 | −11.7 |

**Note**: Underline text indicates the highest three scores for each protein.

bonding in addition to supporting hydrophobic interactions with TYR119 and LEU120 amino acid residues (Figure 8A). Moreover, quercetin, chlorogenic acid, and rosmarinic acid showed also the highest binding affinity scores for IL-1β (−7.8, −9.4, and −9.2 kcal/mol., respectively).[27,41] They revealed the hydrogen bond interactions with ASN108 and MET148 important amino acid residues in the vicinity of the protein active site[43] (Figure 8B). Binding fit to GSK3-β protein active site requires interactions with LYS85 and ASP200 amino acids which are achieved by quercetin and chlorogenic acid through hydrogen bonding and are supported by other several binding forces, rosmarinic acid showed the highest binding energy score for GSK3-β active site (−11.3 kcal/mol.) through several hydrogen bonding and hydrophobic interactions (Figure 8C).On the other hand, several amino acids are important to bind for inhibition of MMP-8, chlorogenic acid effectively binds to HIS201, HIS207, and ARG222 while quercetin and rosmarinic acid bind to LEU160, and ALA161 in addition to ARG222. All these amino acids are also bound by the co-crystallized ligand (Figure 8D). Eventually, the three compounds bind well to the vicinity of the iNOS active site through hydrogen bonding with TYR588, ARG481, and GLU592 (Figure 8E).

## Cell Culture Assays, Determination of Proinflammatory Cytokine

### Cytotoxicity

Human Skin Keratinocyte (Hacat) cells were utilized to assess the safety of the AO-ZnO-NPs-chitosan gel, as shown in Figure 9. After 24 hours of incubation, concentrations of up to 450 µg/mL of AO-ZnO-NPs-chitosan gel showed no cytotoxic effects. The cell viability remained above 82% across all tested concentrations. These results indicate that the *Althaea Officinalis* extract used in the gel formulation did not exhibit any cytotoxic effects. Furthermore, when applied to cells, the AO-ZnO-NPs-chitosan gel exhibited a significant increase in flow, particularly in response to stimuli like acute inflammation or oxidative stress.[44] This suggests that the gel formulation may provide a sustained release of proteins, thereby enhancing their bioavailability even in compromised skin conditions. Given that the components of the formulation are generally considered safe, these findings support the biocompatibility of the AO-ZnO-NPs-chitosan gel when in contact with skin cells.[14,45]

## Effect of AO-ZnO-NPs-CS Gel Treatment on Serum Inflammatory Cytokines Protein Profiles; IL-6, IL-10, IL-1 β, and TNF-α

Wound inflammation, triggered by the presence of LPS, has been linked to changes in inflammatory cytokines. In our previous findings, we observed that treating wounds with *AO*-ZnO-NPs-chitosan gel effectively reduced the levels of IL-6, IL-1β, and TNF-α in response to LPS in vitro.[46,47] In this study, we collected serum samples from rats treated with different interventions three hours after LPS injection to investigate the impact of *Althaea Officinalis* extract or *AO*-ZnO-NPs-chitosan gel on serum cytokine profiles. Comparing *AO-ZnO-NPs*-chitosan gel treatment to AO extract, we observed a significant decrease in the expression of TNF-α, IL-6 and, IL-1β, (33.3%, 25%, and 43.3% respectively compared to the control group) (Figure 10). Additionally, the use of *AO-ZnO-NPs*-chitosan gel led to a notable increase in the serum levels of the anti-inflammatory cytokine IL-10 by 1.9-fold compared to the control group (Figure 10). This finding suggests that the therapy involving *AO*-ZnO-NPs-chitosan gel may be beneficial in addressing wound inflammation, as IL-1β is a key pro-inflammatory mediator in local acute inflammation. Various studies have emphasized the

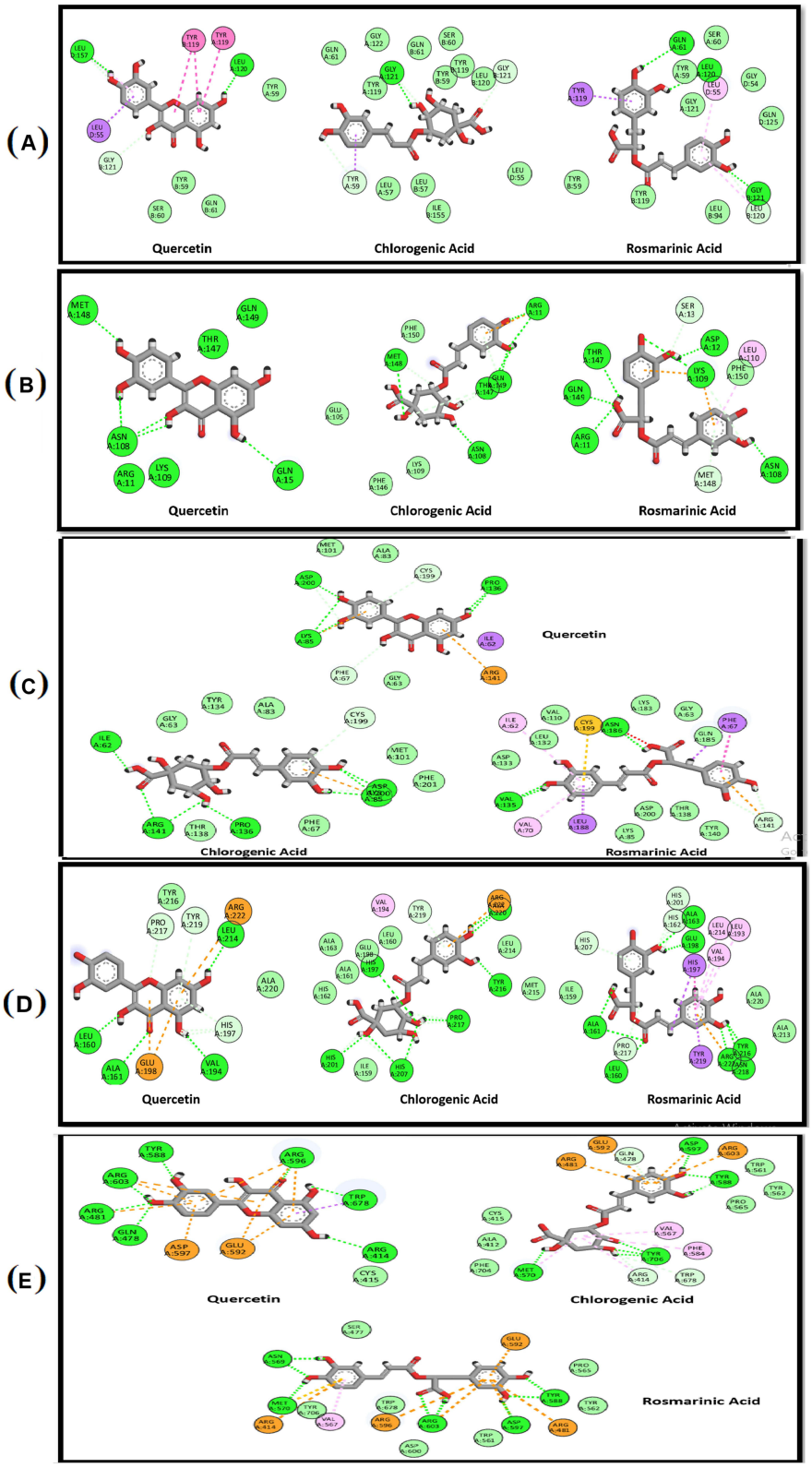


**Figure 8** Binding interactions of quercetin, chlorogenic acid, and Rosmarinic acid (**A**) in TNF-α binding site, (**B**) IL-1β binding site, (**C**) in GSK3-β binding site, (**D**) in MMP-8 binding site and (**E**) in iNOS binding site.


https://doi.org/10.2147/IJN.S455270 DovePress

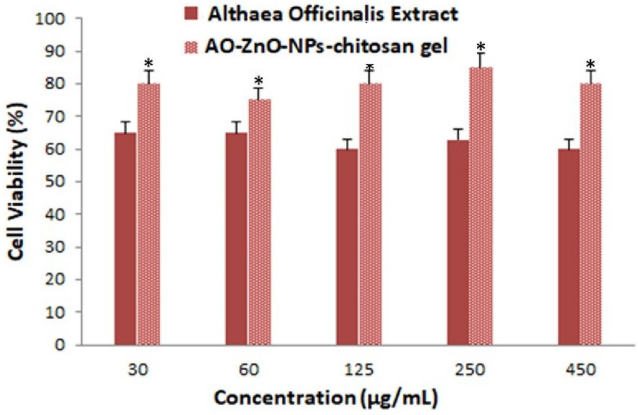


**Figure 9** Cell viability, evaluated by MTT cell proliferation assay, of HSE-2 cells after incubation for 24 h. The experiments were repeated three times for each tested cell line. *$p < 0.005$ versus negative control.

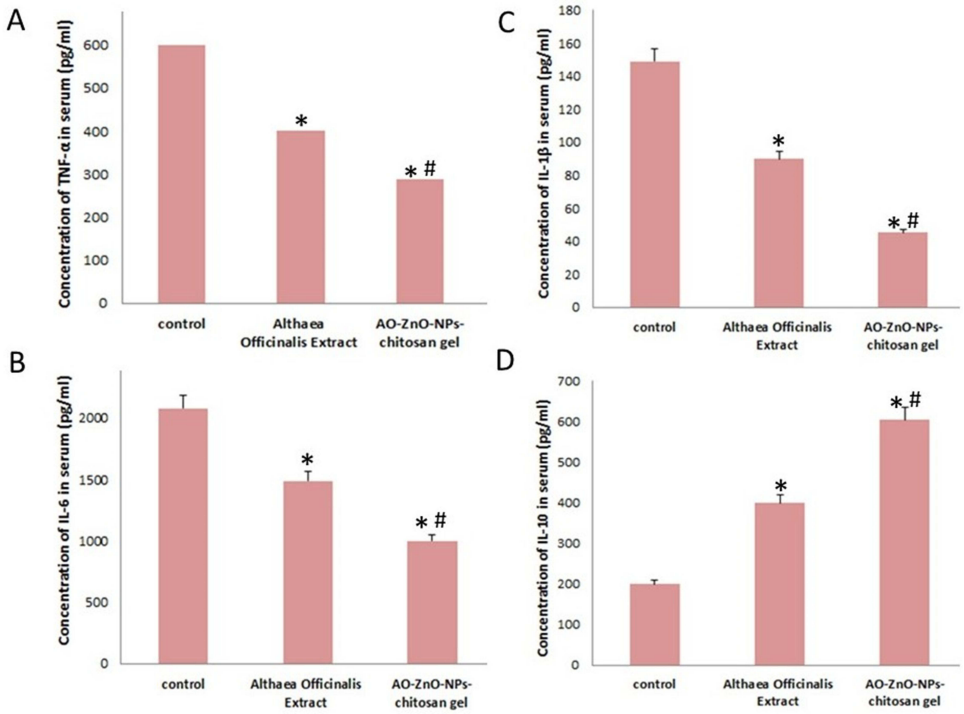


**Figure 10** Effect of *Athlaea Officinalis* extract and *A.O.*-NPs CS gel on serum inflammatory cytokines protein profile; (**A**) TNF-α, (**B**) IL-6, (**C**) IL-1β and (**D**) IL-10. The data are presented as means ± SE (n = 6). Significance *Relative to the control group, #Relative to the *Althaea Officinalis* group.

importance of immunoregulatory cytokines in the inflammatory response of wounds. TNF-α, released early in the inflammatory response, plays a role in regulating the levels of IL-6.[19,48,49] Similarly, IL-1β is an alarm-phase cytokine that is associated with various clinical symptoms related to wounds. Macrophages release IL-10, a significant cytokine that reduces inflammation and modulates the immune system. This is achieved by elevating the levels of the IL-1β receptor antagonist and inhibiting TNF-α (Figure 10). The reduction in LPS-induced wound inflammation, either by promoting IL-10 or inhibiting IL-6, TNF-α, and IL-1β, has been highlighted by previous studies.[44] Our investigation revealed that AO-ZnO-NPs-chitosan gel treatment resulted in a significant decrease in serum levels of IL-6, TNF-α, and IL-1β, along with an increase in IL-10 levels three hours after LPS injection, when compared to *Althaea Officinalis* extract. Therefore, we propose that the modulation of immunoregulatory cytokines is how AO-ZnO-NPs-chitosan gel achieves enhanced therapeutic benefits in wound healing.

## In vivo Study

Figure 11. During the initial stages of wound healing, the application of *A.O*-ZnO-NPs proved to be highly effective due to the antimicrobial and anti-inflammatory effect of zinc oxide nanoparticles and the antiulcer activity of *Althaea officinalis*. Animals treated with *A.O*-ZnO-NPs exhibited a significantly higher percentage of wound healing by the third day of treatment compared to other groups. In contrast, the control medication used for animal recovery showed slow progress. The concentration of the medication, specifically the Chitosan gel of *A.O*.-ZnO-NPs, was found to be around 0.1%. This is based on the understanding that NPs often exhibit improved pharmacokinetic properties, allowing for enhanced therapeutic effects even at lower doses. Therefore, we formulated a 1/10$^{th}$ dose of the drug for its action and conducted a study that yielded the following results. We calculated the percentage of wound contraction by measuring the changes in wound area for each group of animals. Daily observations were made to monitor the evolving alterations of the wound, and wound contraction was noted on the seventh and fourteenth days. While the animals in group I displayed only 22.5% healing due to their natural immune responses, the animals treated with *A.O*-ZnO-NPs (group IV) showed 71.8% healing. Animals treated with Althea Officinalis Extract (group III) displayed 33.1% healing, followed by the animals in the standard treatment group (group II),

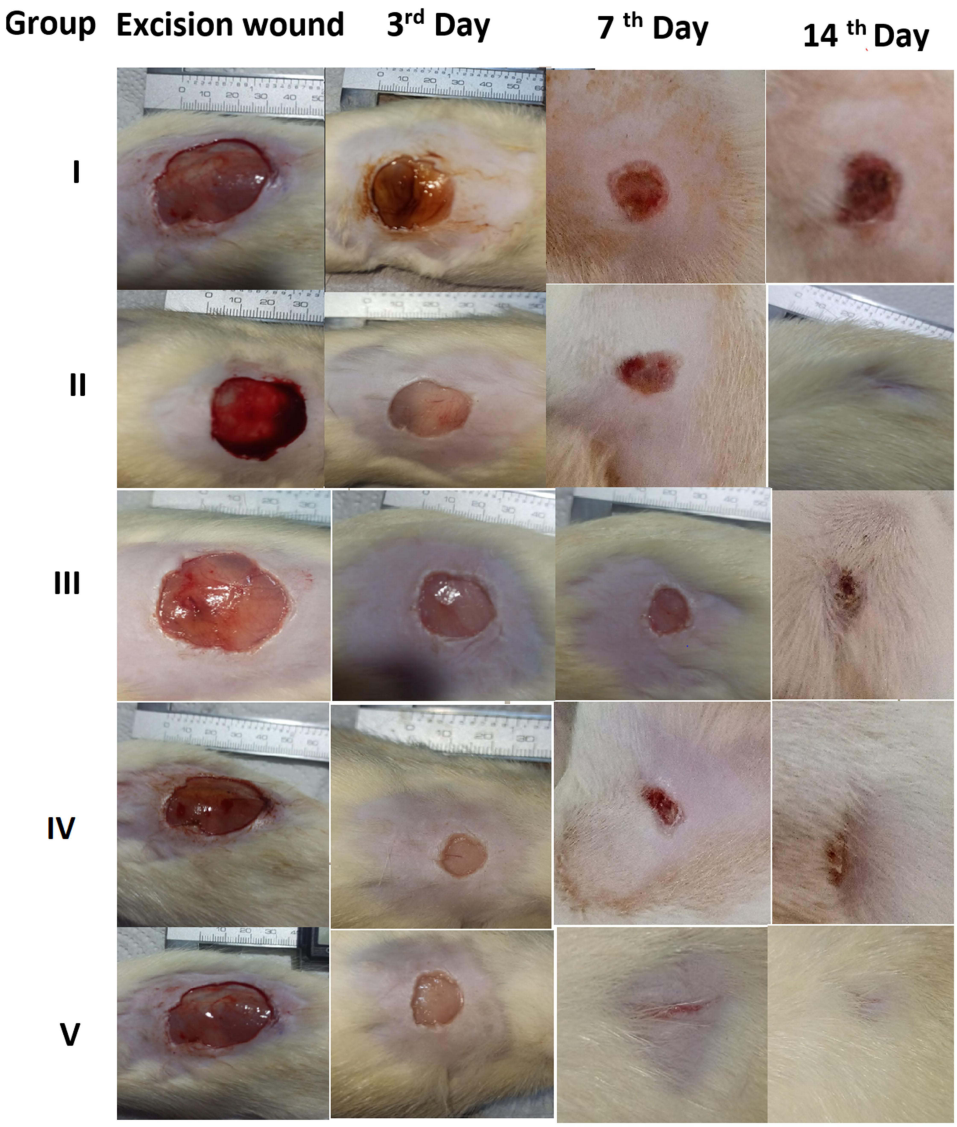


**Figure 11** Comparison of the wound-healing activity of group I (untreated), group II (Mebo +Gentamycin), group III (treated with *Althea Officinalis*), and group IV (treated with *A.O.*–ZnO -NPs) and group V (*A.O.*-ZnO-NPs-Cs) at 3$^{rd}$,7$^{th}$ and 14$^{th}$.

**Table 7** Percentage of Wound-Healing Activity Against a Tested Sample of Groups

| Group | Sample Name | Wound Concentration % Mean ±S.D | | |
|---|---|---|---|---|
| | | 3 rd | 7 th | 14th |
| I | Untreated | 17.1 ± 1.1 | 22.5 ± 0.9 | 28.2 ± 2.1 |
| II | Mebo+ Gentamycin | 39.2 ± 2.1 | 54.1 ± 2.0 | 78.1 ± 1.9 |
| III | Althea Officinalis Extract | 23.1 ± 1.9 | 33.1 ± 0.7 | 42.1 ± 0.9 |
| IV | *A.O.*-ZnO-NPs | 60.2 ± 1.2 | 71.8 ± 0.9 | 80.2 ± 0.7 |
| V | CS- *A.O.*-ZnO-NPs CS gel | 69.3 ± 0.3 | 93.3 ± 1.9 | 98.1 ± 1.2 |

which showed 54.1% healing, as depicted in Figure 11 and Table 7. Group V animals demonstrated 93.3% healing on the seventh day, indicating a complete recovery.[31,50] Images of the wounds from the group treated with CS-*A.O.*-ZnO-NPs gel (group 5) also showed smaller wound sizes on the seventh day.

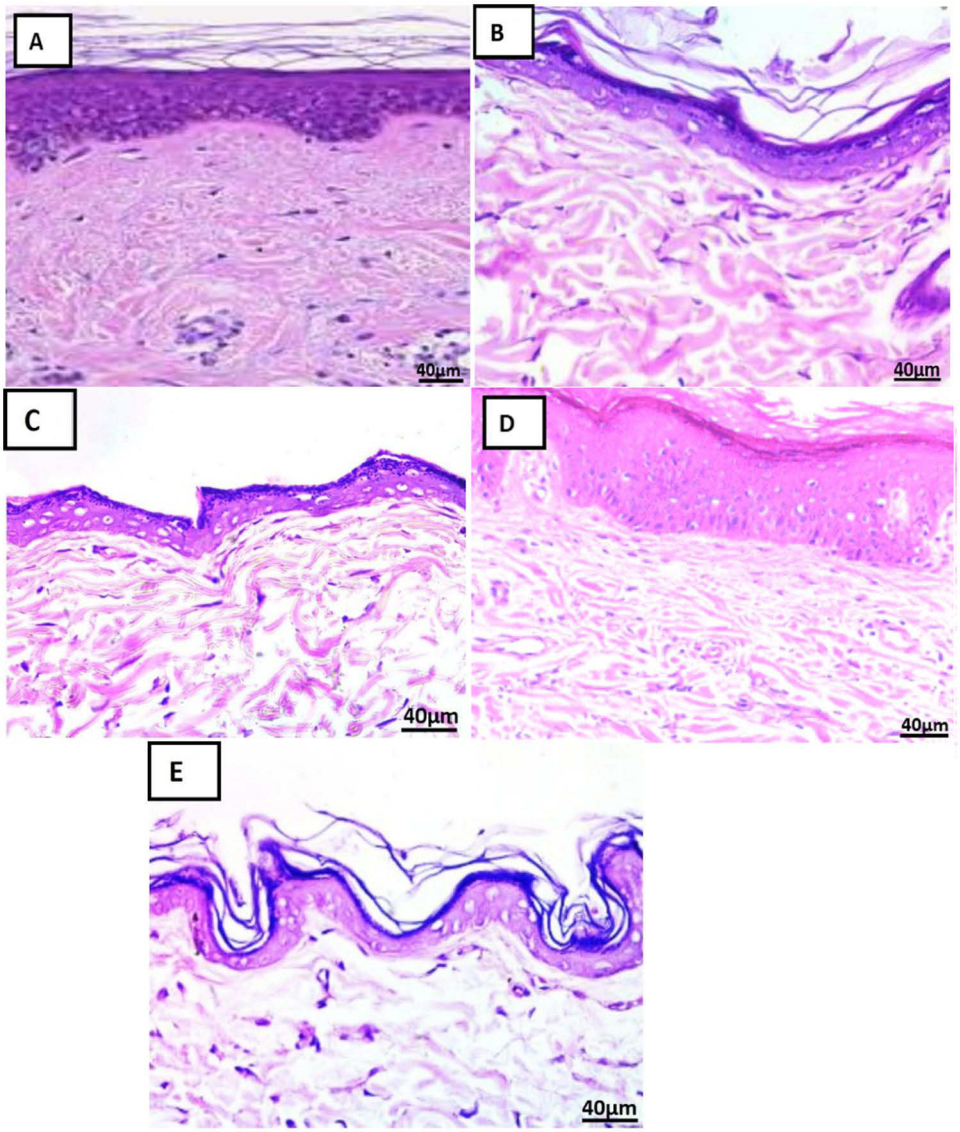


**Figure 12** Photomicrographs of control skin sections of Group (**I**, II, III, IV&V) (H & E x 400) showing (**A–E**) with normal skin histological structural arrangement of dermis and epidermis.

*Althaea Officinalis* with its high concentration of important flavonoid glycosides, phenolic acids, tannins, and flavonoids, exhibits efficacy in the treatment of ulcer and wound healing inflammation. Traditionally, *althaea officinalis* has been used as a gargle for stomach ulcers and mouth and throat ulcers, as well as a treatment for mucous membrane irritation.[7] The flower *Althaea officinalis* is frequently utilized in Middle Eastern folk medicine. Numerous bioflavonoids, vitamins, and antioxidant chemicals can be found in this flower. Strong antioxidant activity was shown by *Althaea officinalis* extract in various antioxidant experiments. It has been shown that *Althaea officinalis* aqueous extract may be useful in treating inflammation and ulcers without causing any obvious side effects.[8] The extract of *Althaea officinalis* has active phytoconstituents such as flavonoids and phenolics, which may be responsible for the gastro-protective effect that has been documented. *Althaea officinalis* possesses both an antioxidant and a mucus-protective (cytoprotection) action.[24] Additionally, the synthesis of zinc oxide nanoparticles (ZnO) has anti-inflammatory, antimicrobial, and wound-healing properties.[44] When combined with CS gel, *A.O*. aqueous extract, and ZnO exhibited significantly better wound healing. these findings are consistent with our earlier study on aqueous extracts of *Althaea officinalis* flowers.

## Histopathology Study

The control histological results: Control skin sections of each Group showing normal skin histological structural arrangement of dermis and epidermis (Figure 12A–E).[51,52]

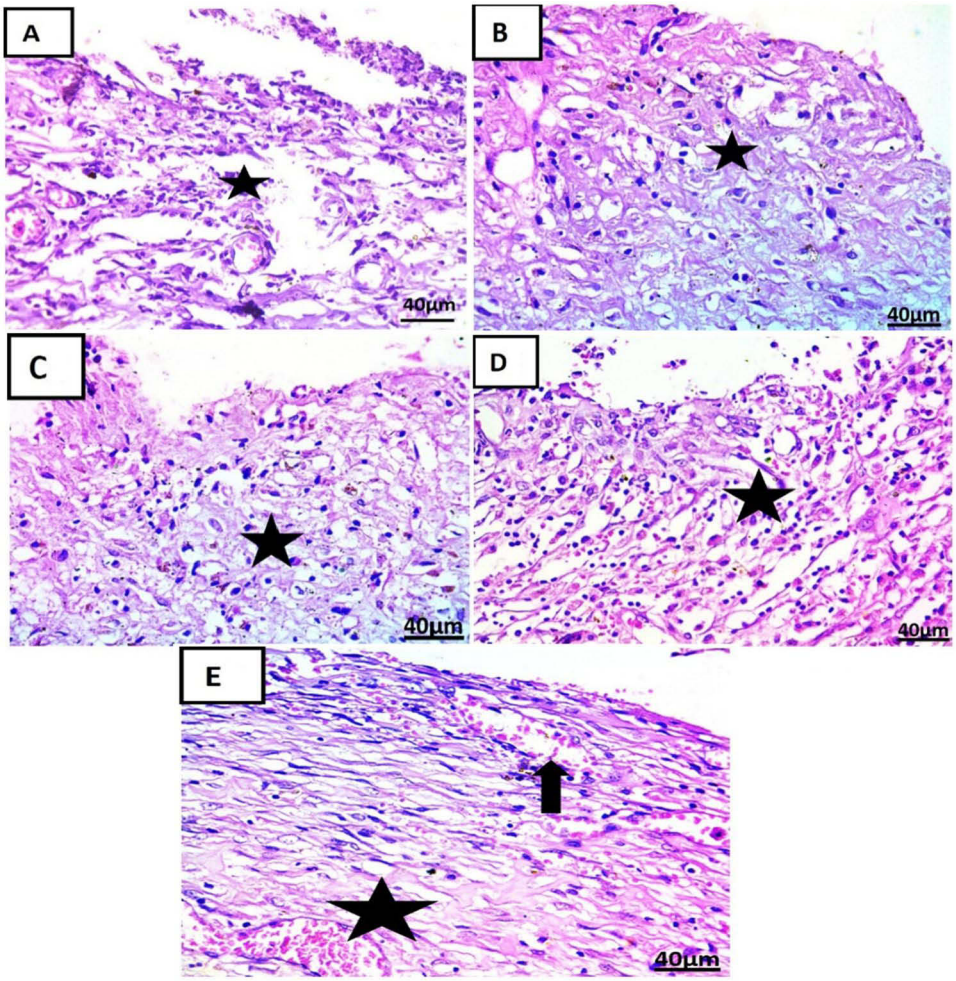


**Figure 13** Photomicrographs of skin sections treatment at 7th day in each group (H & E x 400): (**A**) showing ill-organized fibrous connective tissue with infiltration by mononuclear inflammatory cells (Star). (**B**) showing fibrous connective tissue with infiltration by mononuclear inflammatory cells(star). (**C**) showing fibrous connective tissue formation with infiltration by mononuclear inflammatory cells (star). (**D**) showing fibrous connective tissue formation with mononuclear inflammatory cells and hemorrhage (star). (**E**) showing well-organized fibrous connective tissue with infiltration by mononuclear inflammatory cells (star) and formation of newly formed blood vessels (arrow).

At 3rd day of treatment histological results: Skin sections at 3rd day treatment in each group showing ill-organized fibrous connective tissue with infiltration by mononuclear inflammatory cells (Figure 13A). The appearance of fibrous connective tissue with infiltration by mononuclear inflammatory cells (Figure 13B–D) with the appearance of hemorrhage (Figure 13D). Demonstration of well-organized fibrous connective tissue with infiltration by mononuclear inflammatory cells and formation of newly formed blood vessels (Figure 13E).[17,40–42]

On the 7th day of treatment histological results: Skin sections at 7rd day of treatment in each group showed fibrous connective tissue formation with hemorrhage and infiltration by mononuclear inflammatory cells (Figure 14A). Appearance of well-organized fibrous connective tissue with infiltration by mononuclear inflammatory cells and formation of newly formed blood vessels (Figure 14B). Demonstration of fibrous connective tissue formation with infiltration by mononuclear inflammatory cells (Figure 14C). Appearance of fibrous connective tissue formation with mononuclear inflammatory cells and hemorrhage (Figure 14D). Formation of well-organized fibrous connective tissue with infiltration by mononuclear inflammatory cells covered by some epidermal layer formation (Figure 14E).[53]

On 14th day of treatment histological results: Skin sections at 14th-day treatment in each group showed fibrous connective tissue formation with hemorrhage covered by scab (Figure 15A). Demonstration of well-organized fibrous connective tissue

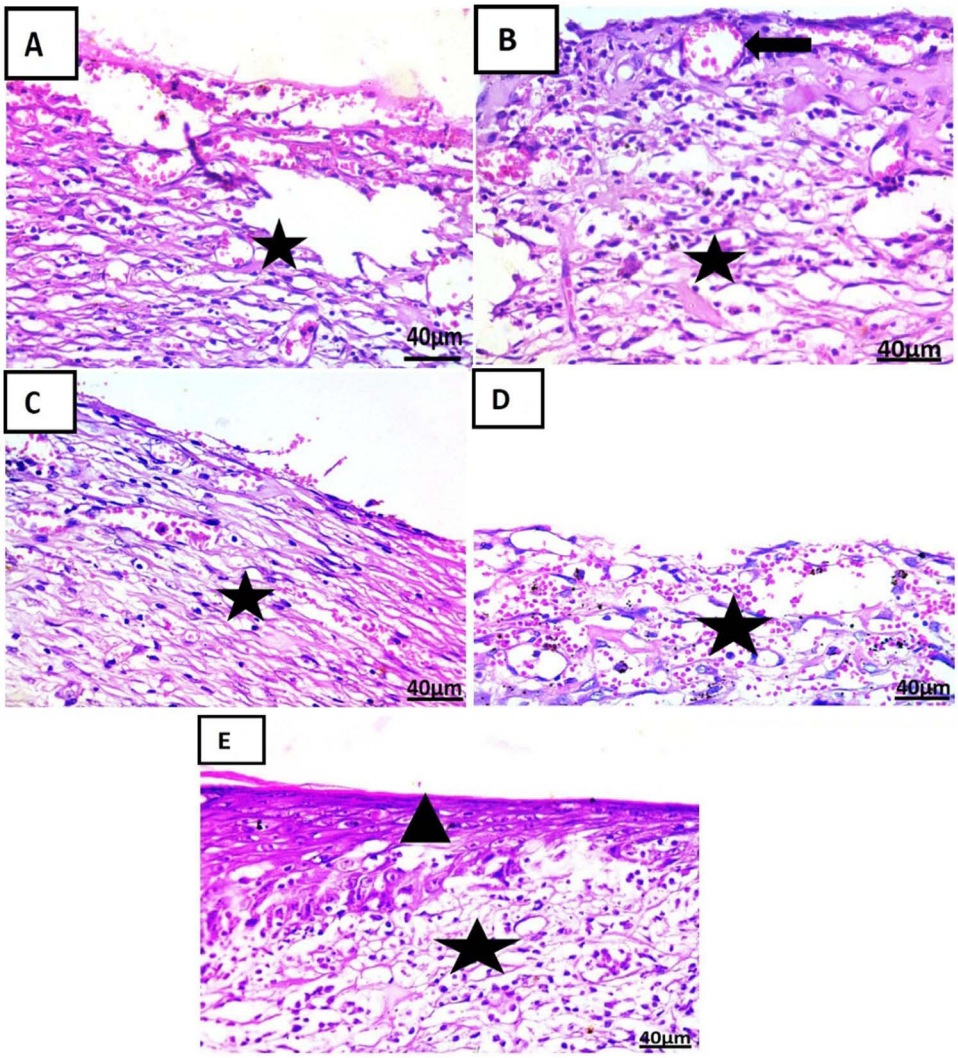


**Figure 14** Photomicrographs of skin sections treatment at 7th day in each group (H & E x 400): (**A**) showing fibrous connective tissue formation with hemorrhage and infiltration by mononuclear inflammatory cells (star). (**B**) showing well-organized fibrous connective tissue with infiltration by mononuclear inflammatory cells (star) and formation of newly formed blood vessels (arrow). (**C**) showing fibrous connective tissue formation with infiltration by mononuclear inflammatory cells (star). (**D**) showing fibrous connective tissue formation with mononuclear inflammatory cells and hemorrhage (star). (**E**) shows the formation of well-organized fibrous connective tissue with infiltration by mononuclear inflammatory cells (star) covered by some epidermal layer formation (arrowhead).

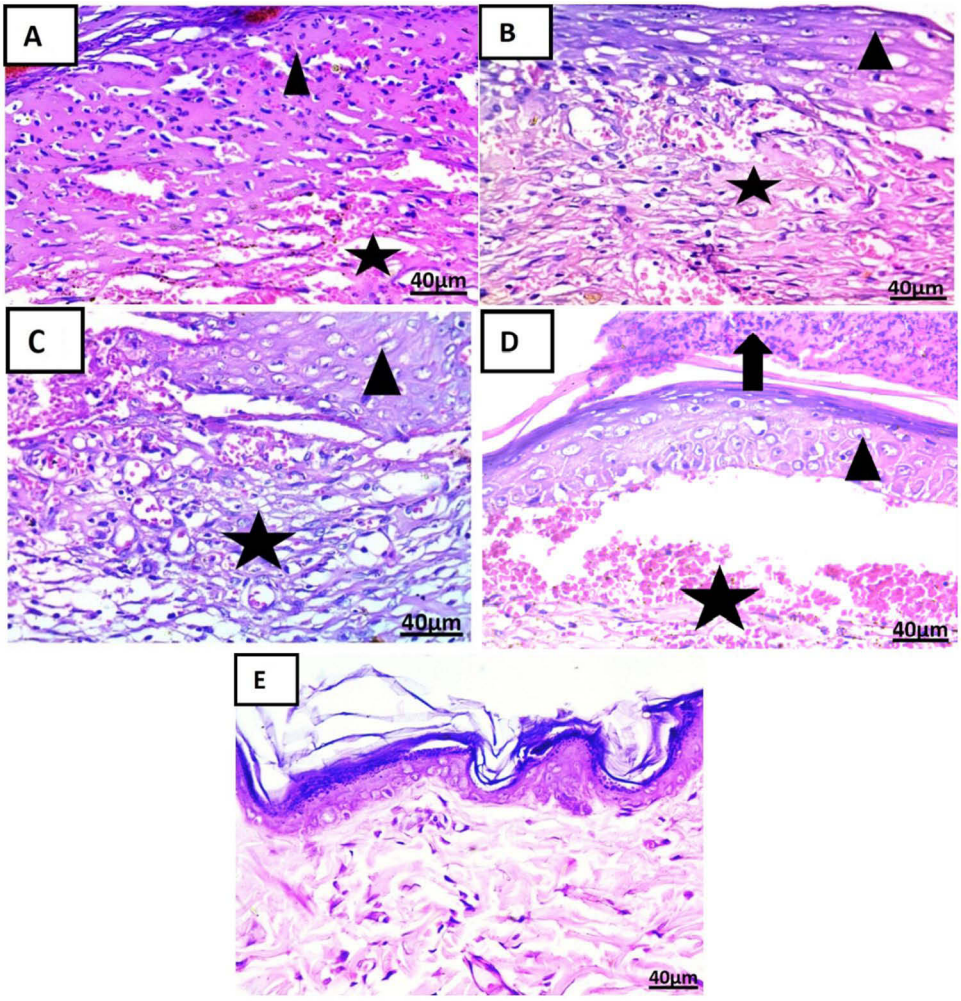


**Figure 15** Photomicrographs of skin sections treatment on the 14th day in each group (H & E x 400): (**A**) showing fibrous connective tissue formation with hemorrhage (star) covered by scab (arrowhead).). (**B**) showing well-organized fibrous connective tissue with infiltration by mononuclear inflammatory cells (star) covered by some epidermal layer (arrowhead). (**C**) showing well-organized fibrous connective tissue with hemorrhage (star) with the partial formation of the epidermis (arrowhead). (**D**) showing fibrous connective tissue formation with hemorrhage (star) and epidermal layer formation (arrow) head) under scab (arrow). (**E**) showing the formation of well-organized fibrous connective tissue covered by the epidermis.

with infiltration by mononuclear inflammatory cells covered by some epidermal layer (Figure 15B). Appearance of well-organized fibrous connective tissue with hemorrhage and partial formation of the epidermis (Figure 15C). Demonstration of fibrous connective tissue formation with hemorrhage and epidermal layer formation under scab (Figure 15D). Formation of well-organized fibrous connective tissue covered by the epidermis (Figure 15E).[17,40–42]

## Conclusions

This study focused on the eco-friendly synthesis of zinc oxide nanoparticles (ZnO-NPs) using *Althaea Officinalis* flowers. These nanoparticles were incorporated into a 2% chitosan gel (CS gel) to create *A.O*-ZnO-NPs CS gel for wound healing. The *Althaea Officinalis* flower extract acted as a reducing agent, and analysis revealed high concentrations of Gallic acid as the most abundant phenolic compound and Quercetin as the most abundant flavonoid compound. The *A.O*-ZnO-NPs were characterized using UV-visible spectroscopy, FTIR, EDX, and TEM analysis, which revealed their spherical, polygonal, and square shapes with a size range of 70–100 nm. The antibacterial potential of the *A.O*-ZnO-NPs CS gel was evaluated against *Staphylococcus aureus, Bacillus subtilis* (Gram-positive) *and Escherichia coli, Pseudomonas aeruginosa* (Gram-negative) using the diffusion agar method. An in-silico study was conducted to identify chemical compounds contributing to wound healing. The results demonstrated improved anti-inflammatory effects with

reduced downregulation of IL-6, IL-1β, and TNF-α in the *A.O*-ZnO-NPs group. In vivo and histopathological analysis further confirmed the ability of the nanoparticles to reduce inflammation and promote wound healing. The developed *A. O*-ZnO-NPs CS gel exhibited significant wound healing activity in diabetic rats, as evidenced by wound contraction measurement and histopathological investigations. This research opens possibilities for utilizing green-synthesized *A.O*-ZnO-NPs and incorporating them into CS gel for drug delivery in wound healing applications.

## Data Sharing Statement

Data sharing is contained in this article.

## Institutional Review Board Statement

The animal study protocol was approved by the animal care and use committee of the Faculty of Medicine, Alexandria University, Egypt (Approval ID: 0306487).

## Funding

This research received no external funding.

## Disclosure

The authors declare no conflicts of interest in this work.

## References

1. Elhabal SF, Elwy HM, Hassanin S, El-Rashedy AA, Hamza AA, Khasawneh MA. Biosynthesis and Characterization of Gold and Copper Nanoparticles from Salvadora Persica Fruit Extracts and Their Biological Properties. *Int J Nanomed*. 2022;17:6095–6112. doi:10.2147/IJN.S385543
2. Borehalli Mayegowda S, Roy A, M NG, et al. Eco-friendly synthesized nanoparticles as antimicrobial agents: an updated review. *Front Cell Infect Microbiol*. 2023;13:1224778. doi:10.3389/FCIMB.2023.1224778
3. Makrynioti D, Zagoriti Z, Koutsojannis C, Morgan PB, Lagoumintzis G. Ocular conditions and dry eye due to traditional and new forms of smoking: a review. *Contact Lens Anterior Eye*. 2020;43(3):277–284. doi:10.1016/j.clae.2020.02.009
4. Mohamed AA, Abu-Elghait M, Ahmed NE, Salem SS. Eco-friendly Mycogenic Synthesis of ZnO and CuO Nanoparticles for In Vitro Antibacterial, Antibiofilm, and Antifungal Applications. *Biol Trace Elem Res*. 2021;199(7):2788–2799. doi:10.1007/S12011-020-02369-4
5. Almutairi B, Albahser G, Almeer R, et al. Investigation of Cytotoxicity Apoptotic and Inflammatory Responses of Biosynthesized Zinc Oxide Nanoparticles from Ocimum sanctum Linn in Human Skin Keratinocyte (Hacat) and Human Lung Epithelial (A549) Cells. *Oxid Med Cell Longev*. 2020;2020:1–9. doi:10.1155/2020/1835475
6. Sumanth B, Lakshmeesha TR, Ansari MA, et al. Mycogenic synthesis of extracellular zinc oxide nanoparticles from xylaria acuta and its nanoantibiotic potential. *Int J Nanomed*. 2020;15:8519–8536. doi:10.2147/IJN.S271743
7. Sutovska M, Capek P, Franova S, et al. Antitussive activity of Althaea officinalis L. polysaccharide rhamnogalacturonan and its changes in Guinea pigs with ovalbumine-induced airways inflammation. *Bratisl Med J*. 2011;112(12):670–675.
8. Albratty M. Design, optimization, and characterization of Althaea officinalis -loaded transliposomes for the treatment of atopic dermatitis: a Box Behnken Design, in vitro, and ex vivo study. *J Biomater Sci Polym Ed*. 2023;34(17):2356–2375. doi:10.1080/09205063.2023.2247879
9. Hage-Sleiman R, Mroueh M, Daher CF. Pharmacological evaluation of aqueous extract of Althaea officinalis flower grown in Lebanon. *Pharm Biol*. 2011;49(3):327–333. doi:10.3109/13880209.2010.516754
10. Abdelfattah DSE, Fouad MA, Elmeshad AN, El-Nabarawi MA, Elhabal SF. Anti-Obesity Effect of Combining White Kidney Bean Extract, Propolis Ethanolic Extract and CrPi3 on Sprague-Dawley Rats Fed a High-Fat Diet. *Nutrients*. 2024;16(2):310. doi:10.3390/NU16020310
11. Manchanda S, Sahoo PK. Topical delivery of Acetazolamide by encapsulating in mucoadhesive nanoparticles. *Asian J Pharm Sci*. 2017;12(6):550–557. doi:10.1016/j.ajps.2017.04.005
12. Khalil M, Hashmi U, Riaz R, Rukh Abbas S. Chitosan coated liposomes (CCL) containing triamcinolone acetonide for sustained delivery: a potential topical treatment for posterior segment diseases. *Int J Biol Macromol*. 2020;143:483–491. doi:10.1016/j.ijbiomac.2019.10.256
13. Matica MA, Aachmann FL, Tøndervik A, Sletta H, Ostafe V. Chitosan as a Wound Dressing Starting Material: antimicrobial Properties and Mode of Action. *Int J Mol Sci*. 2019;20(23). doi:10.3390/IJMS20235889
14. Mohammed MHH, Hamed ANE, Elhabal SF, et al. Chemical composition and anti-proliferative activities of Hyophorbe lagenicaulis aerial parts and their biogenic nanoparticles supported by network pharmacology study. *S Afr J Bot*. 2023;156:398–410. doi:10.1016/J.SAJB.2023.03.018
15. Mohammed MHH, Hamed ANE, Elhabal SF, et al. Metabolic profiling and cytotoxic activities of ethanol extract of Dypsis leptocheilos aerial parts and its green synthesized silver nanoparticles supported by network pharmacology analysis. *S Afr J Bot*. 2023;161:648–665. doi:10.1016/J.SAJB.2023.08.026
16. Hamza AA, Khasawneh MA, Elwy HM, Hassanin SO, Elhabal SF, Fawzi NM. Salvadora persica attenuates DMBA-induced mammary cancer through downregulation oxidative stress, estrogen receptor expression and proliferation and augmenting apoptosis. *Biomed Pharmacother*. 2022;147. doi:10.1016/J.BIOPHA.2022.112666
17. Afrasiabi S, Bahador A, Partoazar A. Combinatorial therapy of chitosan hydrogel-based zinc oxide nanocomposite attenuates the virulence of Streptococcus mutans. *BMC Microbiol*. 2021;21(1). doi:10.1186/S12866-021-02128-Y

18. Elhabal SF, Ghaffar SA, Hager R, et al. Development of thermosensitive hydrogel of Amphotericin-B and Lactoferrin combination-loaded PLGA-PEG-PEI nanoparticles for potential eradication of ocular fungal infections: in-vitro, ex-vivo and in-vivo studies. *Int J Pharm X*. 2023:5. doi:10.1016/J.IJPX.2023.100174
19. Fathy Elhabal S, El-Nabarawi MA, Abdelaal N, et al. Development of canagliflozin nanocrystals sublingual tablets in the presence of sodium caprate permeability enhancer: formulation optimization, characterization, in-vitro, in silico, and in-vivo study. *Drug Deliv*. 2023;30(1):2241665. doi:10.1080/10717544.2023.2241665
20. Al-Shoubki AA, Teaima MH, Abdelmonem R, El-Nabarawi MA, Elhabal SF. Potential application of sucrose acetate isobutyrate, and glyceryl monooleate for nanonization and bioavailability enhancement of rivaroxaban tablets. *Pharm Sci Adv*. 2023;100015. doi:10.1016/J.PSCIA.2023.100015
21. Al-Shoubki AA, Teaima MH, Abdelmonem R, El-Nabarawi MA, Elhabal SF. Sucrose acetate isobutyrate (SAIB) and glyceryl monooleate (GMO) hybrid nanoparticles for bioavailability enhancement of rivaroxaban: an optimization study. *Pharm Dev Technol*. 2023;1–11. doi:10.1080/10837450.2023.2274944
22. Abdelmonem R, Elhabal SF, Abdelmalak NS, El-Nabarawi MA, Teaima MH. Formulation and Characterization of Acetazolamide/Carvedilol Niosomal Gel for Glaucoma Treatment: in Vitro, and In Vivo Study. *Pharmaceutics*. 2021;13(2):1–20. doi:10.3390/PHARMACEUTICS13020221
23. Yilmaz E, Borchert HH. Effect of lipid-containing, positively charged nanoemulsions on skin hydration, elasticity and erythema–an in vivo study. *Int J Pharm*. 2006;307(2):232–238. doi:10.1016/J.IJPHARM.2005.10.002
24. Zaghlool SS, Abo-Seif AA, Rabeh MA, Abdelmohsen UR, Messiha BAS. Gastro-Protective and Anti-Oxidant Potential of Althaea officinalis and Solanum nigrum on Pyloric Ligation/Indomethacin-Induced Ulceration in Rats. *Antioxidants (Basel)*. 2019;8(11). doi:10.3390/ANTIOX8110512
25. Yu X, Wang C, Wang Y, et al. Microneedle Array Patch Made of Kangfuxin/Chitosan/Fucoidan Complex Enables Full-Thickness Wound Healing. *Front Chem*. 2022;10:838920. doi:10.3389/fchem.2022.838920
26. Trott O, Olson AJ. AutoDock Vina: improving the speed and accuracy of docking with a new scoring function, efficient optimization, and multithreading. *J Comput Chem*. 2010;31(2):455–461. doi:10.1002/JCC.21334
27. Eberhardt J, Santos-Martins D, Tillack AF, Forli S. AutoDock Vina 1.2.0: new Docking Methods, Expanded Force Field, and Python Bindings. *J Chem Inf Model*. 2021;61(8):3891–3898. doi:10.1021/ACS.JCIM.1C00203
28. Al-Shoubki AA, Teaima MH, Abdelmonem R, El-Nabarawi MA, Elhabal SF. Potential application of sucrose acetate isobutyrate, and glyceryl monooleate for nanonization and bioavailability enhancement of rivaroxaban tablets. *Pharm Sci Adv*. 2024;2:100015. doi:10.1016/J.PSCIA.2023.100015
29. Sathe P, Saka R, Kommineni N, Raza K, Khan W. Dithranol-loaded nanostructured lipid carrier-based gel ameliorate psoriasis in imiquimod-induced mice psoriatic plaque model. *Drug Dev Ind Pharm*. 2019;45(5):826–838. doi:10.1080/03639045.2019.1576722
30. Nadaban A, Gooris GS, Beddoes CM, Dalgliesh RM, Bouwstra JA. Phytosphingosine ceramide mainly localizes in the central layer of the unique lamellar phase of skin lipid model systems. *J Lipid Res*. 2022;63(9):100258. doi:10.1016/j.jlr.2022.100258
31. Mengie T, Mequanente S, Nigussie D, Legesse B, Makonnen E. Investigation of Wound Healing and Anti-Inflammatory Activities of Solvent Fractions of 80% Methanol Leaf Extract of Achyranthes aspera L. (Amaranthaceae) in Rats. *J Inflamm Res*. 2021;14:1775–1787. doi:10.2147/JIR.S298244
32. Juncan AM, Moisă DG, Santini A, et al. Advantages of Hyaluronic Acid and Its Combination with Other Bioactive Ingredients in Cosmeceuticals. *Molecules*. 2021;26(15):4429. doi:10.3390/MOLECULES26154429
33. Renu S, Shivashangari KS, Ravikumar V. Incorporated plant extract fabricated silver/poly-D,l-lactide-co-glycolide nanocomposites for antimicrobial based wound healing. *Spectrochim Acta A Mol Biomol Spectrosc*. 2020;228. doi:10.1016/J.SAA.2019.117673
34. Herculano RD, Dos Santos TO, de Barros NR, et al. Aloe vera-loaded natural rubber latex dressing as a potential complementary treatment for psoriasis. *Int J Biol Macromol*. 2023;242(February):124779. doi:10.1016/j.ijbiomac.2023.124779
35. Montenegro L, Castelli F, Sarpietro MG. Differential scanning calorimetry analyses of idebenone-loaded solid lipid nanoparticles interactions with a model of bio-membrane: a comparison with in vitro skin permeation data. *Pharmaceuticals*. 2018;11(4):138. doi:10.3390/ph11040138
36. Trombino S, Servidio C, Laganà AS, Conforti F, Marrelli M, Cassano R. Viscosified solid lipidic nanoparticles based on naringenin and linolenic acid for the release of cyclosporine a on the skin. *Molecules*. 2020;25(15):3535. doi:10.3390/molecules25153535
37. Yasser M, El Naggar EE, Elfar N, Teaima MH, El-Nabarawi MA, Elhabal SF. Formulation, optimization and evaluation of ocular gel containing nebivolol Hcl-loaded ultradeformable spanlastics nanovesicles: in vitro and in vivo studies. *Int J Pharm X*. 2024;7. doi:10.1016/J.IJPX.2023.100228
38. Khan R, Mirza MA, Aqil M, et al. In Vitro and In Vivo Investigation of a Dual-Targeted Nanoemulsion Gel for the Amelioration of Psoriasis. *Gels*. 2023;9(2):112. doi:10.3390/gels9020112
39. Feghhi M, Sharif Makhmalzadeh B, Farrahi F, Akmali M, Hasanvand N. Anti-microbial effect and in vivo Ocular Delivery of Ciprofloxacin-loaded liposome through rabbit's eye. *Curr Eye Res*. 2020;1–7. doi:10.1080/02713683.2020.1728777
40. Elmehbad NY, Mohamed NA, Abd El-Ghany NA, Abdel-Aziz MM. Reinforcement of the antimicrobial activity and biofilm inhibition of novel chitosan-based hydrogels utilizing zinc oxide nanoparticles. *Int J Biol Macromol*. 2023;246. doi:10.1016/J.IJBIOMAC.2023.125582
41. Keller A, Chavez JD, Tang X, Bruce JE. Leveraging the Entirety of the Protein Data Bank to Enable Improved Structure Prediction Based on Cross-Link Data. *J Proteome Res*. 2021;20(1):1087–1095. doi:10.1021/ACS.JPROTEOME.0C00495
42. BIOVIA Discovery Studio Visualizer 4.5 – molecular Visualization – my Biosoftware – bioinformatics Softwares Blog. Available from: https://mybiosoftware.com/biovia-discovery-studio-visualizer-4-5-molecular-visualization.html. Accessed November 3, 2023.
43. Asghar MA, Yousuf RI, Shoaib MH, et al. Green Synthesis and Characterization of Carboxymethyl Cellulose Fabricated Silver-Based Nanocomposite for Various Therapeutic Applications. *Int J Nanomed*. 2021;16:5371–5393. doi:10.2147/IJN.S321419
44. Elhabal S, Abdelaal N, Al-Zuhairy S, et al. Revolutionizing Psoriasis Topical Treatment: enhanced Efficacy Through Ceramide/Phospholipid Composite Cerosomes Co-Delivery of Cyclosporine and Dithranol: in-Vitro, Ex-Vivo, and in-Vivo Studies. *Int J Nanomed*. 2024;19:1163–1187. doi:10.2147/IJN.S443812
45. Asasutjarit R, Managit C, Phanaksri T, Treesuppharat W, Fuongfuchat A. Formulation development and in vitro evaluation of transferrin-conjugated liposomes as a carrier of ganciclovir targeting the retina. *Int J Pharm*. 2020;577:119084. doi:10.1016/j.ijpharm.2020.119084
46. Yang X, Tang Y, Wang M, et al. Co-delivery of methotrexate and nicotinamide by cerosomes for topical psoriasis treatment with enhanced efficacy. *Int J Pharm*. 2021:605(April):120826. doi:10.1016/j.ijpharm.2021.120826

47. Wang LC, Okitsu CY, Zandi E. Tumor necrosis factor alpha-dependent drug resistance to purine and pyrimidine analogues in human colon tumor cells mediated through IKK. *J Biol Chem*. 2005;280(9):7634–7644. doi:10.1074/JBC.M413384200
48. Gao J, Chen F, Fang H, Mi J, Qi Q, Yang M. Daphnetin inhibits proliferation and inflammatory response in human HaCaT keratinocytes and ameliorates imiquimod-induced psoriasis-like skin lesion in mice. *Biol Res*. 2020;53(1). doi:10.1186/S40659-020-00316-0
49. Li X, Wang L, She L, et al. Immunotoxicity assessment of ordered mesoporous carbon nanoparticles modified with PVP/PEG. *Colloids Surf B Biointerfaces*. 2018;171:485–493. doi:10.1016/J.COLSURFB.2018.07.072
50. Mäenpää K, Ilves M, Zhao L, Alenius H, Sinkko H, Karisola P. Effects of Superficial Scratching and Engineered Nanomaterials on Skin Gene Profiles and Microbiota in SKH-1 Mice. *Int J Mol Sci*. 2023;24(21):15629. doi:10.3390/IJMS242115629
51. Deana NF, Zaror C, Del Sol M, Bagnato VS, Alves N. Wound contraction rate in excised and unexcised burn wounds with laser photobiomodulation: systematic review and meta-analysis of preclinical studies. *Burns*. 2023;49(2):261–274. doi:10.1016/J.BURNS.2022.05.009
52. Liu Q, Zhang N, Li Z, He H. Efficacy of autologous platelet-rich plasma gel in the treatment of refractory pressure injuries and its effect on wound healing time and patient quality of life. *Clinics*. 2021;76:1–7. doi:10.6061/CLINICS/2021/E2355
53. Alsareii SA, Alzerwi NAN, Alasmari MY, Alamri AM, Mahnashi MH, Shaikh IA. Topical Application of Premna integrifolia Linn on Skin Wound Injury in Rats Accelerates the Wound Healing Process: evidence from In Vitro and In Vivo Experimental Models. *Evid Based Complement Alternat Med*. 2022;2022:1–14. doi:10.1155/2022/6449550